Distributed Antenna Systems in 5G Mobile Communications

Master's thesis 2021

for obtaining the academic degree

Dipl. Ing.

as part of the study

Telecommunications

carried out by

Manuel Lobinger

student number: 01525862

Institute of Telecommunications

at TU Wien

AT-1040 Vienna

Gußhausstraße 25/E389

Main-advisor: Associate Prof. Dipl.-Ing. Dr.techn. Stefan Schwarz

Co-advisor: M.Sc. Charmae F. Mendoza

Code of Conduct

Hiermit erkläre ich, dass die vorliegende Arbeit gemäß dem Code of Conduct – Regeln zur Sicherung guter wissenschaftlicher Praxis (in der aktuellen Fassung des jeweiligen Mitteilungsblattes der TU Wien), insbesondere ohne unzulässige Hilfe Dritter und ohne Benutzung anderer als der angegebenen Hilfsmittel, angefertigt wurde. Die aus anderen Quellen direkt oder indirekt übernommenen Daten und Konzepte sind unter Angabe der Quelle gekennzeichnet. Die Arbeit wurde bisher weder im In– noch im Ausland in gleicher oder in ähnlicher Form in anderen Prüfungsverfahren vorgelegt.

Vienna, October 2021

Manuel Lobinger

Acknowledgements

I would like to express my gratitude to my supervisors Associate Prof. Dipl.-Ing. Dr.techn. Stefan Schwarz and M.Sc. Charmae F. Mendoza for the useful comments, remarks and engagement through the learning process of this thesis. Furthermore, I would like to thank my advisors for introducing me to the topic as well for the support on the way. I would like to thank my loved ones, who have supported me throughout the entire process, both by keeping me harmonious and helping me assemble the pieces.

The financial support by the Austrian Federal Ministry for Digital and Economic Affairs, the Austrian National Foundation for Research, Technology and Development, and the Christian Doppler Research Association is gratefully acknowledged.

Abstract

The needs of mobile communication users increase from year to year, as there are occurring more and more applications using mobile networks. On the one side the demand for high data rates increases, while on the other side reliable low-latency connections are gaining interest, especially in public transport and in the car industry, e. g. autonomous driving. To provide these demands the capacity of future beyond 5th generation (5G) networks has to increase. This is done by using higher carrier frequencies in the range of 3-300 GHz, making use of a lot of unoccupied bandwidth. As this comes with the drawback of higher path loss and worse channel conditions the coverage of beyond 5G networks needs to improve. A possible way to do this is the deployment of distributed antenna systems (DAS). These systems make use of spatially distributed antennas, which are connected with a physical low-latency link to a central unit (CU). This CU is responsible for the coordination of the antennas and does all the signal processing.

This thesis analyses DASs regarding various topics. The thesis starts with the development of a single-user DAS and the used hybrid beamforming is investigated. This includes user grouping based on channel characteristics with a threshold test and a specific grouping algorithm, used for the beamforming. The first part ends with a comparison of a DAS and a macro cell. In the second part, the system model is extended to a multi-user system and the following topics are analyzed. First, the variation of general parameters like the number of antenna array elements and radio frequency (RF) chains are analyzed. After that, a realistic per RF chain power constraint is investigated. Then channel estimation errors are introduced and compared to a codebook-based beamforming strategy and the needed number of feedback bits. Thereafter scheduling aspects are covered. The thesis ends with a comparison of a multi-user DAS to small cells. All mentioned aspects were implemented and simulated with the Vienna 5G System Level Simulator.

Kurzfassung

Die Anforderungen von Mobilfunk Benutzern steigen von Jahr zu Jahr, durch die steigende Anzahl an Anwendungen die eine Internetverbindung über das Mobilfunknetz benötigen. Zum einen werden immer höhere Datenraten verlangt, zum anderen werden höchst zuverlässige Verbindungen benötigt, wie zum Beispiel im öffentlichen Verkehr oder in der Automobilindustrie, beispielsweise zur Unterstützung des autonomen Fahrens. Um diesen Anforderungen gerecht zu werden müssen künftige 5G Netze höhere Kapazitäten liefern. Damit diese Kapazitäten erreicht werden kommen höhere Frequenzen, im Bereich von 3- 300 GHz zum Einsatz. Dies ermöglicht die Benützung bislang unerschlossener Frequenzbänder. Da aber mit höheren Frequenzen auch höhere Pfadverluste und schlechtere Kanaleigenschaften mit einhergehen, müssen zukünftige Mobilfunknetze bessere Netzabdeckung bereitstellen. Eine Lösung um dies zu erreichen sind verteilte Antennensysteme. Hier werden mehrere Antennen in derselben Zelle geografisch verteilt und physikalisch mit einer zentralen Einheit verbunden. Diese Einheit koordiniert die Antennen und ist für die Signalverarbeitung zuständig.
Diese Diplomarbeit beschäftigt sich mit verschiedenen Themen aktueller Mobilfunknetze, unter Verwendung verteilter Antennensysteme. Zu Beginn wird ein Einzelbenutzersystem konzipiert und das verwendete hybride Beamforming wird analysiert. Dies beinhaltet die Gruppierung mehrerer Benutzer mittels Schwellentest und einem speziellen Gruppierungsalogrithmus, auf Basis ihrer Kanaleigenschaften. Zum Schluss des ersten Teiles wird ein verteiltes Antennensystem mit einer herkömmlichen Makrozelle verglichen. Im zweiten Teil wird das System auf ein Mehrbenutzersystem erweitert und folgende Themen bearbeitet. Als Erstes wid das Verhalten des Systemes bei variierenden Parametern, wie zum Beispiel der Anzahl von Antennen Elementen oder Hochfrequenzkanälen, analysiert. Im Anschluss wird eine realistische Leistungsbeschränkung eingeführt, die die Leistung pro Hochfrequenzkanal beschränkt. Danach wird das System mit Kanalschätzfehler behaftet und dessen Auswirkung analysiert. Weiters wird das Thema Scheduling behandelt und der resultierende Kompromiss zwischen Datenrate und Latenz gezeigt. Am Ende der Diplomarbeit wird ein verteiltes Antennensystem mit mehreren Kleinzellen verglichen. Alle Modelle sind mit dem Vienna 5G System Level Simulator implementiert und simuliert worden.

Contents

1 Introduction

1.1 Motivation

As the traffic demand of communication network users increases, with every new application that has evolved in the past years and is considered in the future, e.g. online games, high resolution video streams or car-to-x (C2X) communications, the mobile data traffic is doubled every year [1]. With this statement in mind Qualcomm forecasts that beyond 5th generation (5G) networks have to provide a 1000 times higher capacity than the current networks [2]. To achieve this, research is focusing on the exploration of millimeter wave (mmWave) technologies, in the frequency range of 3GHz to 300GHz. This step to higher frequencies allows the usage of a lot of unoccupied bandwidth. However, this advantage comes with the increase of path and fading losses, which means channel conditions get worse. For 5G networks research proposed multiple solutions for this problem. One answer is the use of multiple-input-multiple-output (MIMO) systems, like antenna arrays (AA) with beamforming (BF) techniques, such as digital or analog BF [3]. The idea behind this is, that multiple antennas, called antenna elements, are grouped to an array and each antenna element transmits the same signal with a phase-shift, so that all signals are perfectly superposed at the receiver. This leads to a so-called beam, which has a gain proportional to the number of antenna elements, called BF gain. While digital BF is flexible and can form a high number of different beams, this approach is highly expensive due to the need of radio frequency (RF) chains, for each antenna element. RF chains contain e.g. analog-to-digital converters, digital-to-analog converters, power amplifiers and mixers. Analog BF reduces these costs, by only using one RF chain and phase shifters for the BF, but then only one beam is possible. A third possibility, called hybrid BF, combines the digital and analog approach to perform close to optimal, compared to digital BF, while keeping the costs low.
Another solution to improve the coverage of the cellular network is densification with smaller cells, which means the provider of the cellular network would need to increase the number of base stations, by inserting micro cells in the existing network. Measurement campaigns in New York City at 28 GHz showed, that for consistent coverage the cell radius of a base station needs to be 100-200m [4][5]. A second way of improving coverage would be the deployment of a distributed antenna system (DAS). In this architecture multiple antennas are distributed geographically in the cell and are connected with a low latency fiber to the base station. With this it is possible to overcome path loss and shadowing effects because the transmitting antennas are closer to the users. The main differences to the micro cell approach is that a DAS still needs only one base station and each user can be served by geographically distributed antennas, making use of spatial diversity. DASs are widely known and used in indoor scenarios to cover deadspots of coverage [6], but in the last years research gained more and more

interest to consider DASs also in outdoor scenarios for 5G networks.

1.2 Objectives

In my thesis I analyse the performance of a DAS, combined with the technologies of hybrid BF, in terms of signal-to-noise ratio (SNR) or signal-to-interference-plus-noise ratio (SINR) and throughput. A crucial part of my thesis is to implement the needed features in the Vienna 5G System Level Simulator [7] and develop a full multi-user capable system. In the first part of my thesis I implement and analyse BF from simple analog BF to fully-connected hybrid BF in a single-user DAS. The following topics are included:

- Cluster users with similar channel conditions and serve them with an analog beamformer
- Cluster users with similar channel conditions and serve them with a hybrid beamformer
- Compare a centralized antenna to a DAS

The second part is to extend the system model to a multi-user DAS and to investigate the following topics on a system level perspective:

- Multiplexing - how many users can be served in parallel with the same total power?
- How do power constraints affect the performance of hybrid BF?
- To which extent cause channel estimation errors a reduction of the achievable SINR? How many bits are required in a feedback based system for the BF?
- What is the trade-off between low latency and the achievable throughput?
- How does a DAS perform compared to a small cell structure?

2 State of the art

In this chapter I provide an overview of the main topics of my thesis, according to current literature. In Sec. 2.1 I cover the basics of DASs and in Sec. 2.2 I talk about BF. At the end I introduce the Vienna 5G System Level Simulator in Sec. 2.3, to explain how my simulations are done.

2.1 Distributed Antenna Systems

DASs are widely known and used to improve coverage in indoor environments [8][9]. Architecture, furniture and walls inside of buildings can be a major problem for wave propagation, leading to a problematic multi path propagation environment [10]. In a DAS remote antenna units (RAU) are distributed throughout the building, reducing the distance from the users to the antennas, which improves the channel characteristics by reducing path loss and fading effects. RAUs are only used for transmitting and receiving signals, hence have no signal processing capabilities by themselves. Therefore deploying another RAU is not as complex as using another basestation. All RAUs are connected to a central unit (CU), which processes all signals. Another advantage is that we can easily control the interference between signals transmitted from different RAUs, since all signals are generated at the CU. This is more complicated in small cell systems, where interference coordination requires information exchange between small cells. In Fig. 2.1 I show the architecture of a in-building DAS from [11]. They analysed the performance of a DAS with frequency reuse in each floor, dependent on the user position. According to [11] interference was not only considered through penetration of the floors but also through reflections from a nearby building.

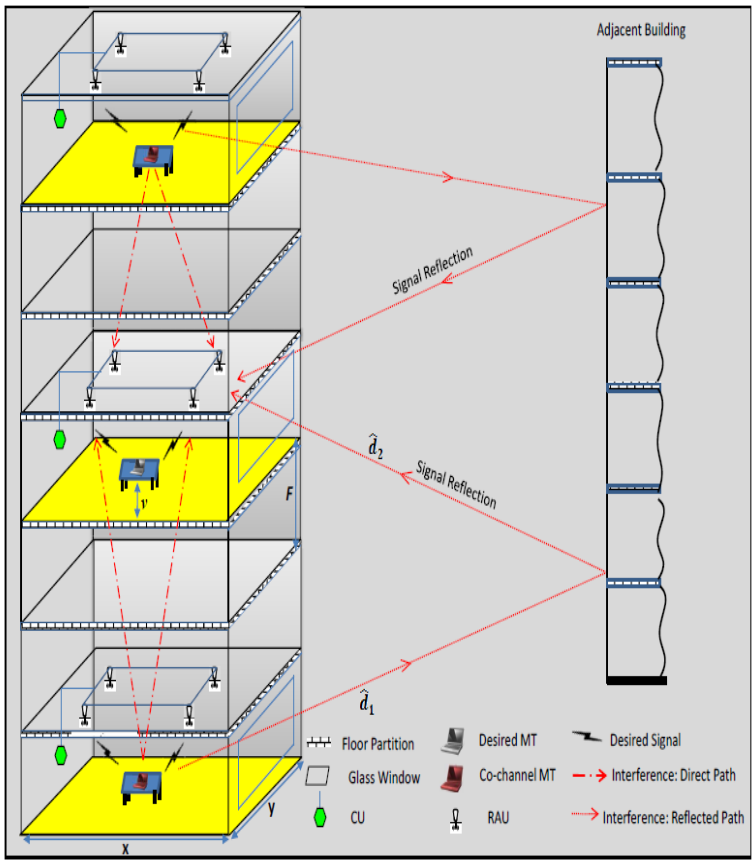

Figure 2.1: In-Building DAS, Source: [11, Figure 1] ©2013 IEEE.

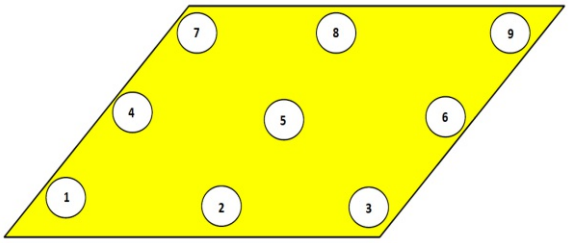

Figure 2.2: User positions, Source: [11, Figure 2] ©2013 IEEE.

Fig. 2.3 shows the results of [11] in terms of average spectral efficiency over signal-to-noise ratio (SNR). N' denotes the number of RAUs that are used to serve the user, E_s is the transmit symbol energy and N_0 is the noise spectral density. $\frac{E_s}{N_0}$ is then the transmit SNR. In total there are four RAUs in each floor and always the strongest

RAUs are selected.

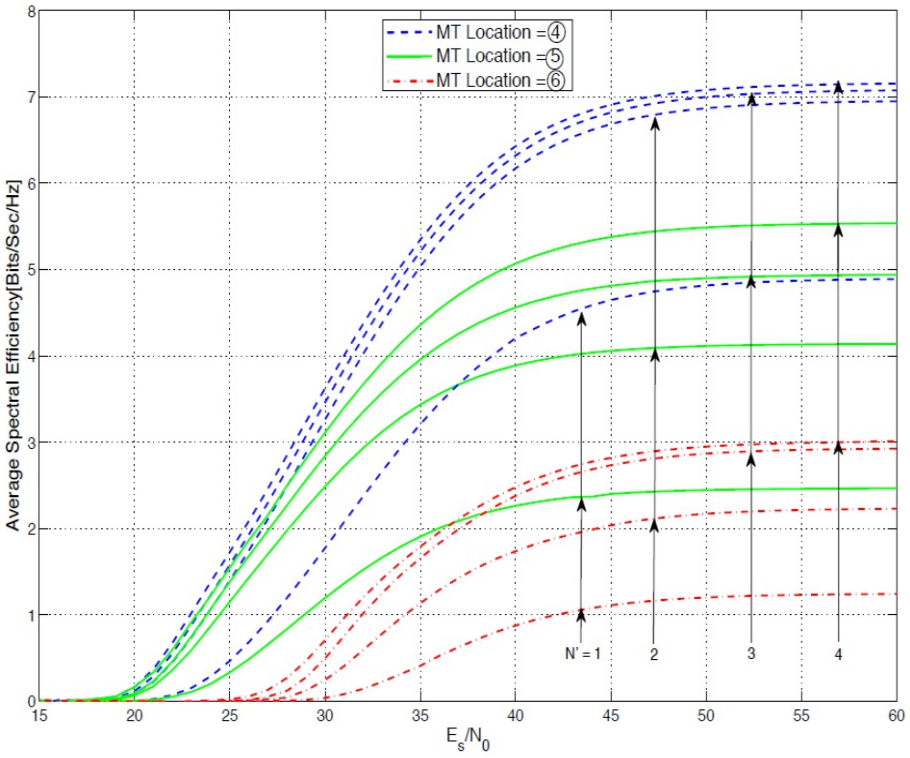

Figure 2.3: Spectral efficiency for different user positions, Source: [11, Figure 5] ©2013 IEEE.

These results show, that the spectral efficiency varies dependent on the users position, shown in Fig. 2.2. This is due to higher interference at positions closer to the window. Also the needed number of RAUs change with the position of the user. On the left side on the floor only two RAUs are necessary to perform almost the same as four RAUs. While in the middle of the floor all RAUs should be used for transmission. The saturation at high SNR can be explained by the increasing interference. This limits the SINR even though the SNR increases.
DASs have gained more and more attention as one possibility, to overcome the high losses, coming from the necessary increase of frequency to the range of mmWaves [12] also in outdoor scenarios. Also a possible solution would be the deployment of smaller cells, namely micro, pico or femto cells. The authors of [13] already compared a DAS with a micro cell structure. In Fig. 2.4 I show the structure of seven macro cells split into sectors, where each sector corresponds to a micro cell.

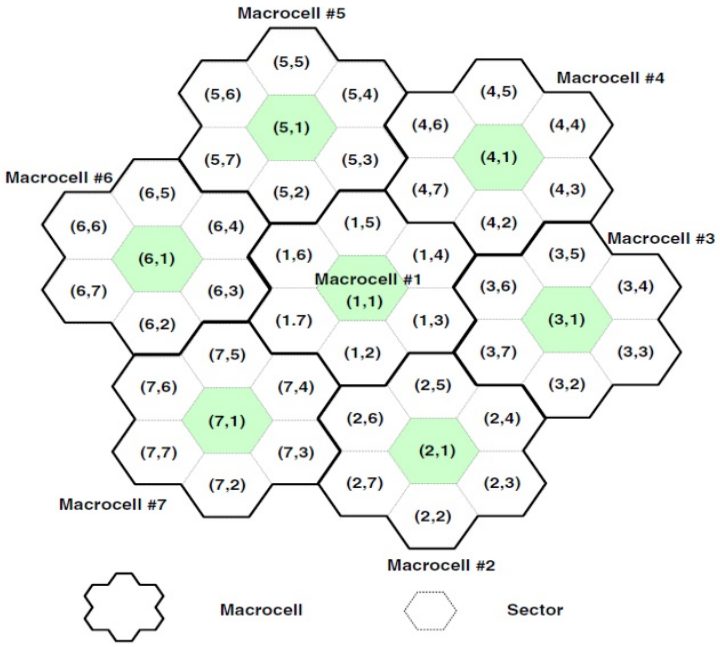

Figure 2.4: Macro cell structure, Source: [13, Figure 1] ©2011 IEEE.

The same frequency is re-used for every sector with equal second digit, e.g. (1,1) and (5,1) use the same frequency. This is highlighted by the green shaded areas. The re-use factor, defined as $\frac{1}{M}$, equals $\frac{1}{7}$ for a micro cell structure because one macro cell is split into seven micro cells.

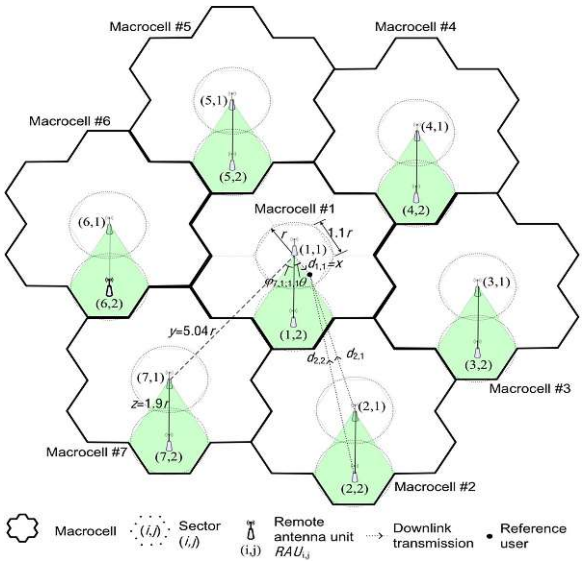

(a) $\frac{1}{M} = \frac{1}{6}$

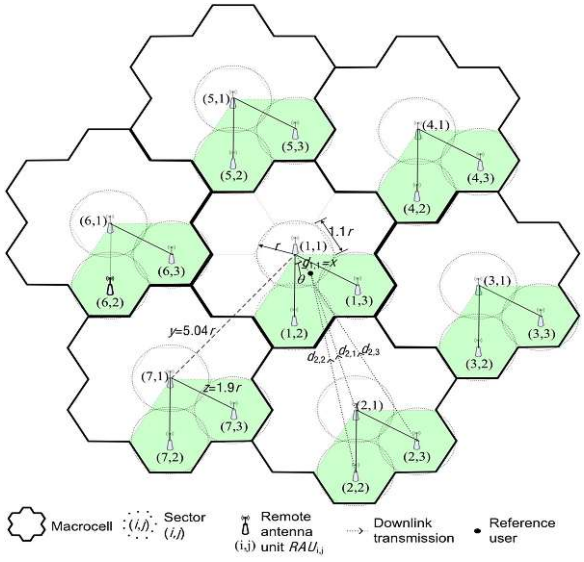

(b) $\frac{1}{M} = \frac{1}{3}$

Figure 2.5: Frequency re-use patterns in a DAS, Source: [13, Figure 4,5] ©2011 IEEE.

Fig. 2.5 shows the same concept with a DAS for every macro cell, where instead of splitting the macro cell into several micro cells, each sector uses one RAU.
Again the green shaded areas mark the areas, where the same frequencies are used. Fig. 2.5a and Fig. 2.5b show the frequency re-use pattern for $\frac{1}{M} = \frac{1}{6}$ and $\frac{1}{M} = \frac{1}{3}$, respectively. In case of a DAS, increasing the re-use factor also increases the number

of RAUs, which serve one user. For $\frac{1}{M} = \frac{1}{6}$ up to two RAUs, and for $\frac{1}{M} = \frac{1}{3}$ up to three RAUs can transmit the same signal to the user. This means in case of $\frac{1}{M} = \frac{1}{6}$ the central and one outer RAU would transmit the signal and for $\frac{1}{M} = \frac{1}{3}$ the central and two outer RAUs would transmit the signal. Higher re-use factors are leading to higher inter-channel interference but by transmitting the same signal over multiple RAUs you also gain spatial diversity.

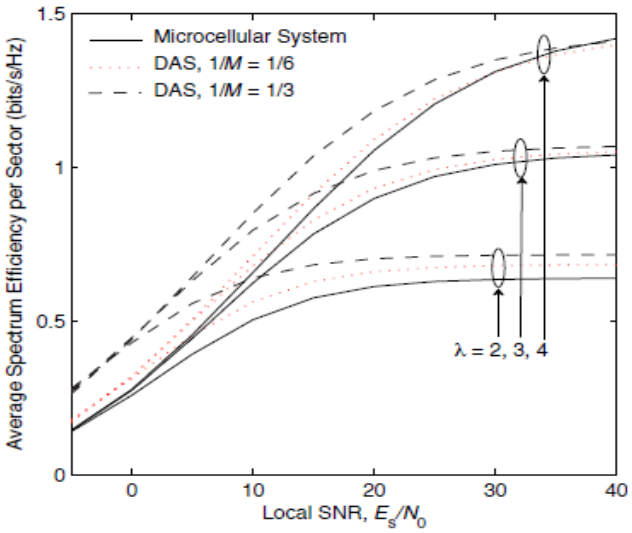

Figure 2.6: Spectral efficiency comparison of a microcellular system and a DAS with different frequency re-use factors for multiple path loss exponents λ, Source: [13, Figure 8] ©2011 IEEE.

In Fig. 2.6 you can see the comparison of a DAS with a micro cell structure in terms of spectral efficiency from [13]. It shows, that a DAS outperforms micro cells, due to a trade-off between inter-channel interference and spatial diversity gain.

2.2 Beamforming

MIMO techniques are seen as key features for future 5G and beyond networks, enabling BF with AAs, to increase spectral efficiency and overcome high path losses from mmWaves [14]. The principle behind BF is that multiple antennas transmit the same signal with defined phase-shifts, so that all signals are coherently superposed at some points in space. This leads to a directional antenna gain pattern, illustrated in Fig. 2.7, called beam. C is a processing unit, which calculates and applies the phase shifts for a given steering angle θ. The antenna gain of this beam is proportional to the number of antennas.

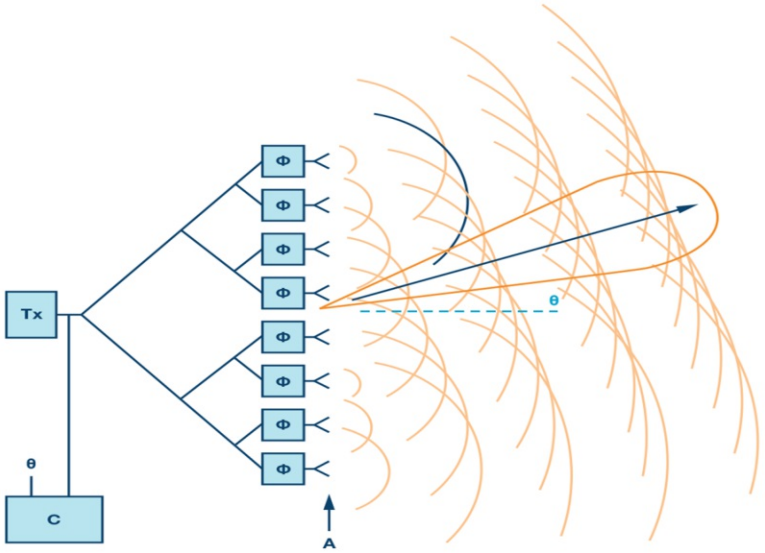

Figure 2.7: Beamforming with an antenna array.

In the simplest form this is done in RF band with phase-shifters, allowing one beam per AA, namely analog BF. The advantage of analog BF is that it only needs one RF chain, which keeps the costs low, but has the disadvantage that only one beam is possible at a time. The counterpart to analog BF is digital BF. In this case the BF is done in baseband (BB) in the digital domain. This requires a RF chain for each antenna element, which is simultaneously the biggest disadvantage of digital BF, leading to high costs in acquisition and operation. The advantage of digital BF is, that the processing in BB enables the possibility of a high number of beams and features like inter-user interference cancellation in multi-user systems. Hybrid BF, as a combination of both forms digital and analog BF, has gained much interest in the recent years [15]. The idea behind hybrid BF is to limit the amount of used RF chains and connect them in a distinct architecture to phase-shifters, which are then connected to every antenna element. With this, it is possible to find a compromise between costs and achievable performance. There are two common architectures for hybrid BF, namely fully-connected and sub-connected. Both structures are shown in Fig. 2.8. In the case of fully connected hybrid BF, each RF chain is connected to all antenna elements N_t, resulting in $N_{RF}N_t$ phase-shifters in total, where N_{RF} is the number of RF chains. For sub-connected hybrid BF, each RF chain is only connected to a subset of $\frac{N_t}{N_{RF}}$ antenna elements, creating a sub-array structure. While the fully-connected structure can make use of the full beamforming gain, because each RF chain transmits the signal over all antenna elements, it also has a high implementation complexity, due to the high number of phase-shifters. The sub-connected structure reduces the number of needed phase-shifters by $\frac{1}{N_{RF}}$ to N_t, but also reduces the beamforming gain by that factor.

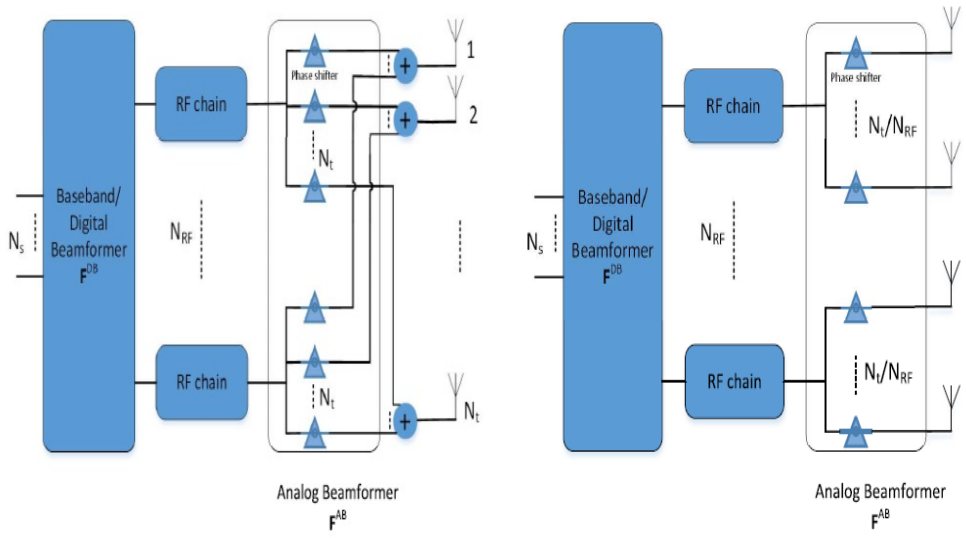

(a) Fully-connected (b) Sub-connected

Figure 2.8: Hybrid BF architectures, Source: [15, Figure 4] ©2011 IEEE.

Research community already developed and compared many hybrid BF strategies on basis of link level simulations for a small amount of users, almost reaching the performance of fully digital BF [16]. Also first studies were made on hybrid BF with co-located and distributed antennas showing a significant increase in spectral and energy efficiency [17].

2.3 Vienna 5G System Level Simulator

Today's cellular networks are complex constructs, based on an orthogonal-frequency-division-multiplexing (OFDM) system. OFDM is a multi-carrier modulation, consisting of multiple orthogonal subcarrier signals. Each subcarrier can be modulated with its own modulation scheme, without interfering each other, due to orthogonality. This allows to schedule users in time and frequency. In order to achieve realistic results one needs to define base stations, users, antennas and the available resources from the used OFDM system, as well as the allocation of these resources to the users. To manage all of these parts of the system, a simulator is required, that is capable of abstracting all of these features. Due to my workship at the Institute of Telecommunications at the Technical University Wien, I am using one of the Vienna Cellular Communications Simulators (VCSS), implemented in Matlab [18], for my thesis. As my focus lies on system level analysis I chose to work with the Vienna 5G System Level Simulator (SLS) [7]. The simulator provides results based on Monte-Carlo simulations. This means many

realizations of a given scenario are simulated and averaged, resulting in an average network performance. This may include different user positions and channel realizations. Fig. 2.9 shows a brief overview of the SLS structure. In a typical simulation, first the scenario is created by placing base stations and users, choosing channel and path loss models and initializing all relevant parameters. After that the main simulation loop gets executed and all results are collected in a last post processing step.

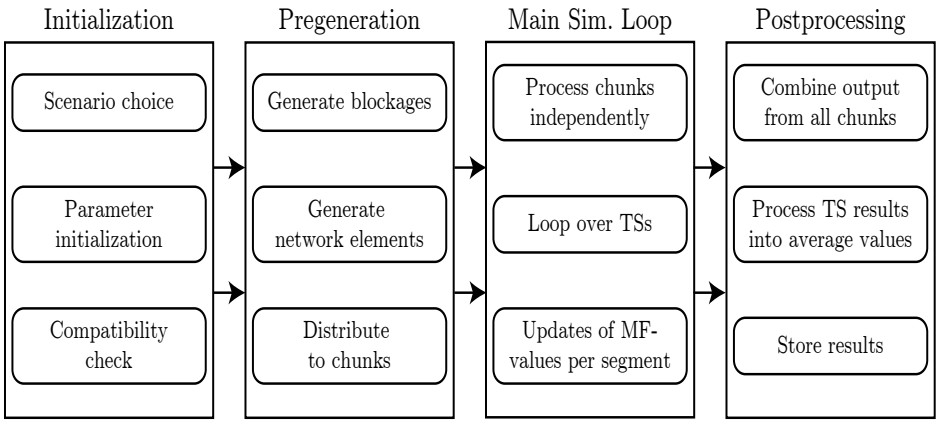

Figure 2.9: Simulator overview, Source: [7] user manual.

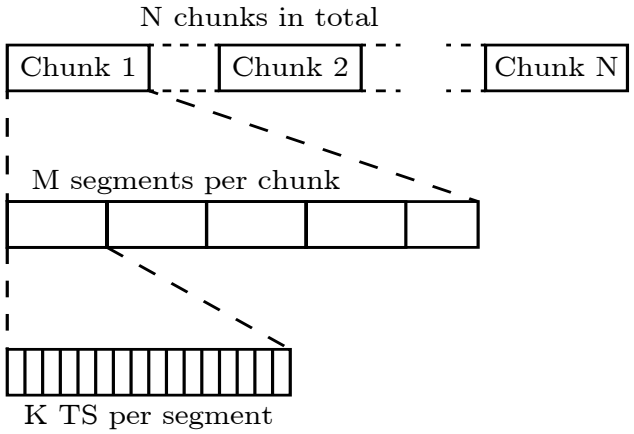

Figure 2.10: Simulator time line, Source: [7] user manual.

In Fig. 2.10 you can see the time line of the SLS, consisting of chunks, segments and time slots (TS). TSs are the smallest time instance in the simulator and are the base for the main simulation loop. In each TS microscopic fading gets updated according to the used channel model and is assumed to be constant within a TS. The length of a

TS can be set in the initialization process and is chosen as 1 ms in all my simulations, representing a LTE-A subframe [19]. Similar to that, in each segment, macroscopic fading is constant. Note that the number of segments is not a changeable parameter, because it depends on the chosen scenario and settings. For example, the simulation of a static user would only have one segment, because macroscopic path loss will not change, if the user is not moving. Each chunk consists of a fixed number of TSs and all necessary data is independent for every chunk. Therefore chunks are used for parallelization to save computation time.

System level simulations are used to see how a whole network performs and all the network elements interact with each other. Such simulations usually consist of multiple base stations and antennas, and hundreds of users. This may include assignment and scheduling strategies for the given resources. Therefore, the simulation of every connection between a user and a basestation on a physical link level perspective, is not feasible, due to the high computational effort. To overcome this problem abstraction models are used to provide results, like bit-error-rate (BER) or throughput, with sufficient detail. These abstraction models are gathered with the Vienna 5G Link Level Simulator (LLS). The calculation process is done in two steps. In the first step all necessary data is collected via the link quality model (LQM) to calculate SINR, illustrated in Fig. 2.11. This includes macroscopic fading through the network layout in terms of path loss, microscopic fading, called small scale fading, in terms of channel realizations and scheduling information in terms of precoders, necessary for the BF, and resource allocation.

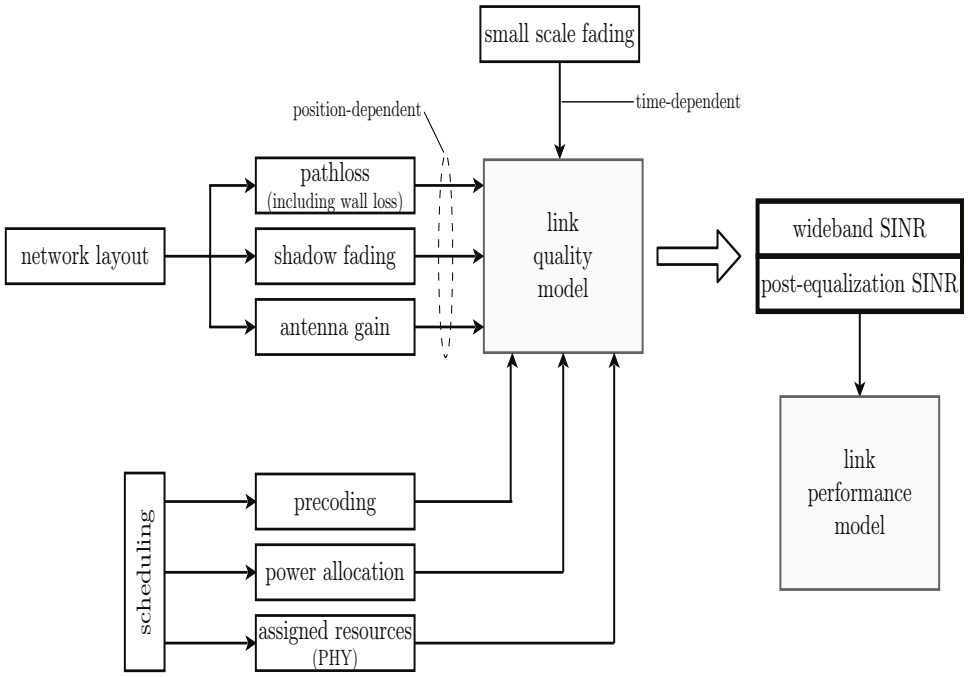

Figure 2.11: Link Quality Model, Source: [7] user manual.

Scheduling is the decision, which users are provided with data in a given TS. Resource allocation means, which user is served by how many and which subcarriers of the OFDM system. Based on the LTE-A standard twelve subcarriers and seven OFDM symbols are grouped to a resource block (RB), which defines the basic scheduling unit. This means in each TS users get scheduled and the available RBs are then distributed among these users. The number of scheduled users depends on the used scheduling strategy. Anything between all or only one user of the total user list is possible.
The output of the LQM is called a resource grid and is depicted in Fig. 2.12. This grid represents a three-dimensional matrix, where the axis are the available resources per TS. These are the RBs (nRBFreq), the RB time (nRBTime) and the transmission layers (nLayers). Due to implementation complexity I am limiting the number of layers, also called data streams, to one in single-user (SU) scenarios and use them as a measure for frequency re-use in multi-user (MU) scenarios. SU scenario means, that each RB can only be assigned to one user, whereas in MU scenarios multiple users can be assigned to the same RB. In MU scenarios severe interference can occur in terms of inter-user-interference, therefore an interference cancellation strategy needs to be applied, which will be covered in a later chapter. This resource grid contains two RBs in time, because I chose the TS length to match a LTE-A subframe. For a typical bandwith of $20\,\mathrm{MHz}$ and a subcarrier spacing of $15\,\mathrm{kHz}$ there are 100 RBs in frequency. This leads to a total of 200 RBs per TS. Due to the current state of the SLS scheduling is always done equally for both RBs in time.

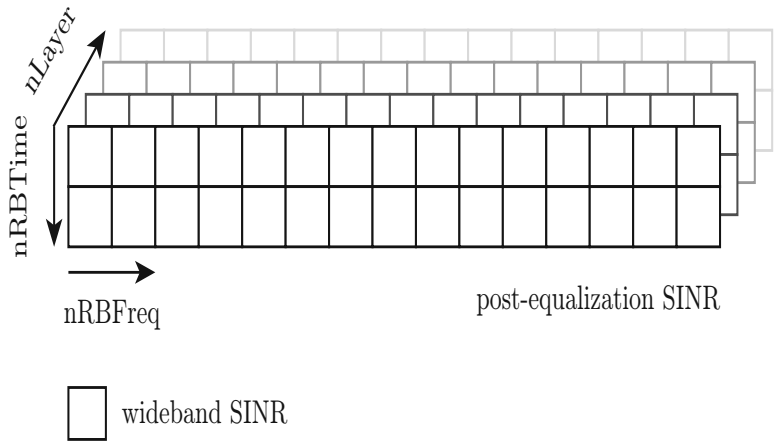

Figure 2.12: Resource grid, Source: [7] user manual.

The post-equalization SINR is calculated for every RB. Fig. 2.13 shows the transmission chain used for the calculation. Each block represents a matrix with the given dimensions. The baseband and analog precoders correspond to the BF matrices needed for hybrid BF. The architecture is chosen as fully-connected as already shown in Fig. 2.8a. The channel consists of microscopic and macroscopic fading in terms of path loss and channel realization of the used channel and path loss models. In the current version of the SLS the receiver contains one receive antenna and uses a zero-forcing (ZF) filter. The output of the receive filter is then the post-equalization SINR. The exact formular for the SINR calculation is given in the system models of the subsections of chapter 3 and 4.

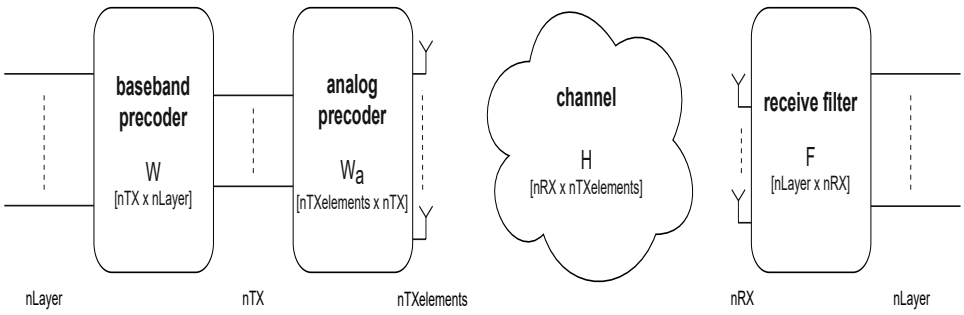

Figure 2.13: Transmission chain, Source: [7] user manual.

The second step is the calculation of the throughput with the link performance model (LPM). This is done by mapping the post-equalization SINR to a channel-quality-indicator (CQI), which then defines the modulation scheme that is used. In table 2.1 all possible CQI values and modulation schemes can be found.

Table 2.1: CQI table, Source: [20, Table 7.2.3-1].

CQI	modulation	code rate x 1024	modulation order	efficiency
0	none	0	0	0
1	QPSK	78	2	0.1523
2	QPSK	120	2	0.2344
3	QPSK	193	2	0.3770
4	QPSK	308	2	0.6016
5	QPSK	449	2	0.8770
6	QPSK	602	2	1.1758
7	16QAM	378	4	1.4766
8	16QAM	490	4	1.9141
9	16QAM	606	4	2.4063
10	64QAM	466	6	2.7305
11	64QAM	567	6	3.3223
12	64QAM	666	6	3.9023
13	64QAM	772	6	4.5234
14	64QAM	873	6	5.1152
15	64QAM	948	6	5.5547

The mapping of SNR/SINR to CQI is done with the BLER curves from Fig. 2.14. These results are simulated with the LLS with the values from Tab. 2.1. The mapping is done by comparing the actual SNR with the decision boundaries. The decision boundaries are defined by a fixed BLER and the corresponding SNR. For this I used the default value of the simulator $\text{BLER}_{max} = 0.1$, which defines the maximum BLER that can occur independent of the CQI. The only exception would be $\text{CQI} = 0$, because then no data is transmitted at all.

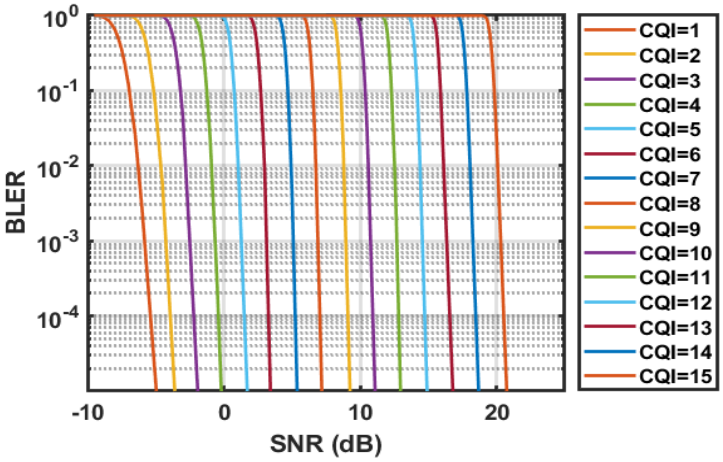

Figure 2.14: SINR to CQI mapping.

When the actual CQI is known, the correct block error ratio (BLER) is chosen from a lookup table. The throughput in bit is then calculated with Eq. (1).

$$\text{ReceivedSymbols} = \text{DataSymbolspRB} \cdot \text{AssignedRBs} \cdot (1 - \text{BLER}) \tag{1}$$

The number of data symbols is calculated with the standardization of LTE-A already mentioned. This is twelve symbols in frequency and seven symbols in time per RB. In addition each RB reserves twelve reference symbols for timing and channel estimation. This leads to

$$\text{DataSymbolspRB} = 12 \cdot 7 - 12 = 72. \tag{2}$$

At the end the achieved throughput in bit is calculated according to the modulation scheme defined by the CQI value.

$$\text{Throughput} = \text{ReceivedSymbols} \cdot \text{ModOrder} \cdot \text{CodeRate} - \text{CRCBits} \tag{3}$$

ModOrder and CodeRate are taken from Tab. 2.1. Eq. (3) also takes bits into account that are used for a cyclic redundancy check (CRC). In the SLS $CRCBits = 24$.

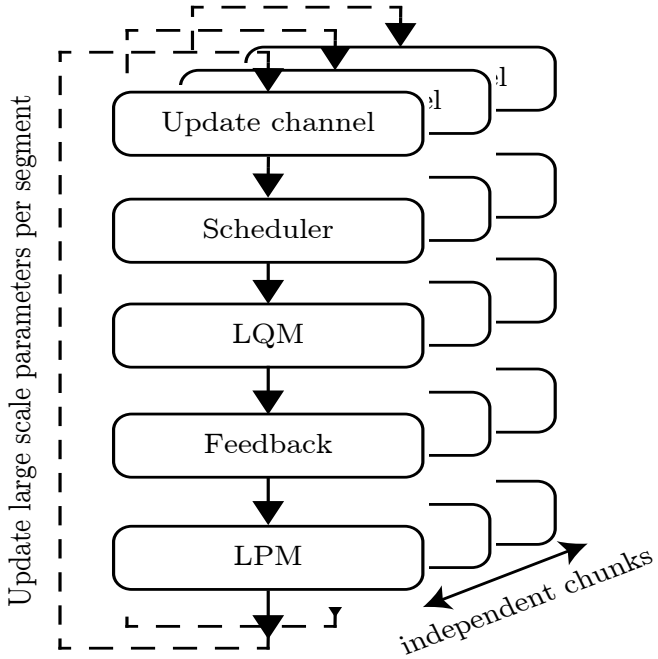

Figure 2.15: Simulation loop, Source: [7] user manual.

To summarize the simulation Fig. 2.15 shows the simulation loop. At the beginning of every TS the microscopic fading is updated and in case the current TS starts a new segment the macroscopic fading is updated. Then the scheduler chooses the scheduled users and assigns the RBs. After that the LQM calculates the post-equalization SINR and with that the LPM calculates the achievable throughput. All of this is repeated for every TS.

3 Single-user analysis

In this chapter I build the system model for hybrid BF for distributed antenna systems step by step and analyse the performance of various user clustering methods. At first I study the basic behaviour of a threshold test with analog BF. Then I extend my simulation model to hybrid BF and analyse an adapted grouping algorithm based on [21]. In the last section the model is extended further to allow the usage of multiple distributed antennas and a realistic scenario with one RAU in the center and with four distributed RAUs is analysed. Each RAU is equipped with a uniform linear antenna array (ULA). The whole section is based on the single-user assumption, which means that each resource block available is only assigned to a single-user. Additionally I assume perfect channel knowledge. The simulations parameters are listed in Tab. 3.1, which are valid for the whole chapter.

Table 3.1: Simulation parameters.

Carrier frequency	2 GHz
System bandwidth B	20 MHz
Subcarrier spacing	15 kHz
Number of resource blocks N_{RB}	100
Channel model	Rayleigh fading
Simulation time	1000 slots

3.1 Threshold test for analog beamforming

My first study is on how a threshold test affects the performance of analog BF. The principle here is to group users with similar channel conditions and form a beam that fits them all. To analyse the basic behaviour of analog BF I chose a scenario with one RAU with $N_{elements}$ antenna elements, which means I can form one beam for one group of users in each time slot. For such a scenario the received signal of user u is defined as

$$y_u = \sqrt{P_u}\mathbf{h}_u^{\mathsf{H}}\mathbf{P}_{RF}\, x + n \tag{4}$$

$$P_u = \xi_u P_{RB} \tag{5}$$

where x defines the unit power transmit signal. $\mathbf{h}_u \in \mathbb{C}^{N_{elements} \times 1}$ is the channel vector from user $u \in \mathcal{S}$, with $\mathcal{S}$ being the set of scheduled users. P_u is the received power

with the path loss $\xi_u \in \mathbb{R}$ and the transmit power per RB $P_{RB} \in \mathbb{R}$. To calculate P_{RB} the total transmit power $P_{tx} \in \mathbb{R}$ is equally distributed over the RBs, with $P_{RB} = \frac{P_{tx}}{N_{RB}}$. $\mathbf{P}_{RF} \in \mathbb{C}^{N_{elements} \times 1}$ is the RF BF vector, also called precoding vector, and $n \sim \mathcal{N}(0, \sigma_n^2)$ is the additive noise, where the noise power σ_n^2 is determined by the thermal noise spectral density and the RB bandwidth.
This leads to a SNR defined as

$$\mathrm{SNR}_u = \frac{\left\| \sqrt{P_u} \mathbf{h}_u^{\mathsf{H}} \mathbf{P}_{RF} \right\|^2}{\sigma_n^2}. \tag{6}$$

Before the RF precoding vector can be defined, one needs to find the users that are getting scheduled. For this a threshold test is used, to find users that have similar channel conditions. At first a reference user has to be chosen. This is done by finding the user with the maximum channel gain

$$\mathbf{h}_r = \max_{k \in \mathcal{U}} \|\mathbf{h}_k\|, \tag{7}$$

where $\mathcal{U}$ is the set of all users. After this the threshold test is done by calculating the correlation of the channel of the reference user and the channels of all other users in $\mathcal{U}$

$$\gamma_k = \frac{\left| \mathbf{h}_r^{\mathsf{H}} \mathbf{h}_k \right|}{\| \mathbf{h}_r \| \cdot \| \mathbf{h}_k \|}, \tag{8}$$

and compare the correlation to the threshold value α. Each user that meets the threshold is then put in the set

$$\mathcal{S} = \{k \mid \gamma_k \geq \alpha, k \in \mathcal{U}\}. \tag{9}$$

All users in $\mathcal{S}$ are getting equally scheduled over all available resource blocks N_{RB}. For $|\mathcal{S}| > N_{RB}$, the users get scheduled over multiple TS. With the set $\mathcal{S}$ of scheduled users, the RF precoder can be calculated as

$$\mathbf{h}_{RF} = \frac{\sum_{u \in \mathcal{S}} \mathbf{h}_u}{|\mathcal{S}|}, \tag{10}$$

$$\mathbf{P}_{RF} = \frac{\mathbf{h}_{RF}}{\|\mathbf{h}_{RF}\|}, \tag{11}$$

which is the maximum ratio transmission (MRT) precoder for the averaged channel of the chosen users. The reason why one precoder needs to be defined for all users is, that due to the usage of phase-shifters the RF precoder is not frequency selective and can not be changed for different RBs. This is why only one beam can be formed with analog BF. In Sec. 3.2 I introduce the baseband precoder, which is capable of forming multiple beams, dependent on the number of used RF chains.

3.1.1 Simulations

In my simulations I used a transmit power $P_{tx} = 40$W and the number of users $|\mathcal{U}| = 200$. To make sure I can highlight the BF gain in my results, I have chosen to use a fixed path loss $\xi_u = 110$ dB for every user. Important here is only that every user has the same path loss and not the actual value. Choosing a higher or lower path loss would just move the SNR result curves in one or the other direction but the relation between them would stay the same. The threshold test and the RF precoder calculation is repeated in every time slot of the simulation.

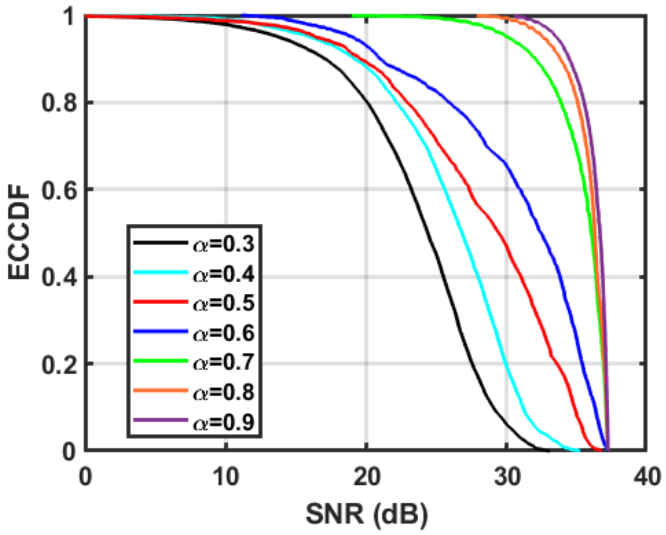

Figure 3.1: ECCDF of SNR for different values of the threshold α for $N_{elements} = 16$.

Fig. 3.1 shows the empirical complementary cumulative distribution function (ECCDF) of SNR for different values of α. You can clearly see the increase in SNR, with increasing α. This is, because higher threshold values lead to a smaller number of users meeting the threshold, and therefore a better fitting beam for each user. The reduction of scheduled users for increasing α can be seen in Fig. 3.2. Note that this can be a problem in terms of latency, because users need to wait longer until they are scheduled again, when only a small number of users is scheduled per TS.
In Fig. 3.3 you see the ECCDF of SNR for a fixed $\alpha = 0.5$, but with varying number of array elements $N_{elements}$. The curves show similar behaviour as in Figure 3.1, namely increasing the number of array elements results in a higher SNR, but in this case this has two reasons. Reason one is that with increasing number of array elements the beam of the RF precoder gets sharper and lesser users meet the threshold, although α stays the same. And the second reason is, with more array elements the precoding gain gets higher. By comparing Fig. 3.3 with Fig. 3.1, you see that increasing the number

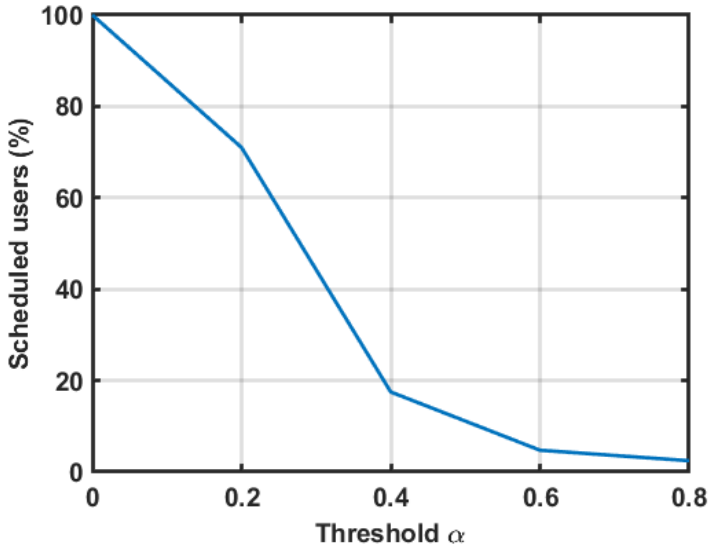

Figure 3.2: Amount of scheduled users over threshold α for $N_{elements} = 16$.

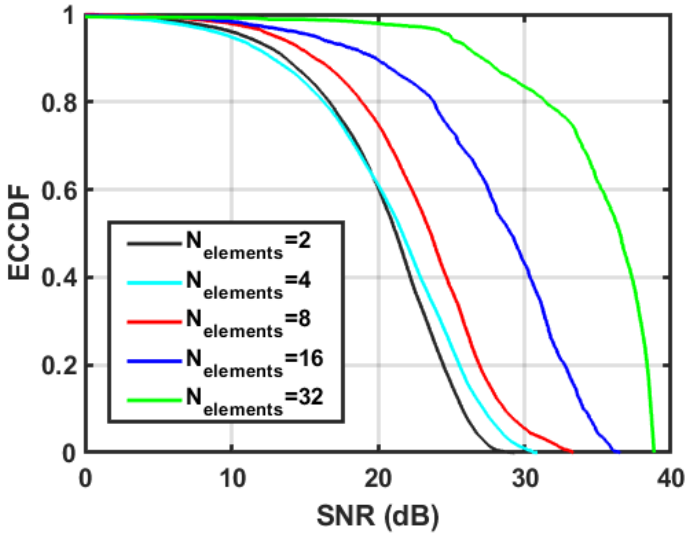

Figure 3.3: ECCDF of SNR for different antenna elements, $\alpha = 0.5$.

of array elements, leads to a more distinct increase of SNR, due to the effect of the precoding gain.
Fig. 3.4 shows the number of scheduled users over array elements, which is, as mentioned above, decreasing for higher number of $N_{elements}$.

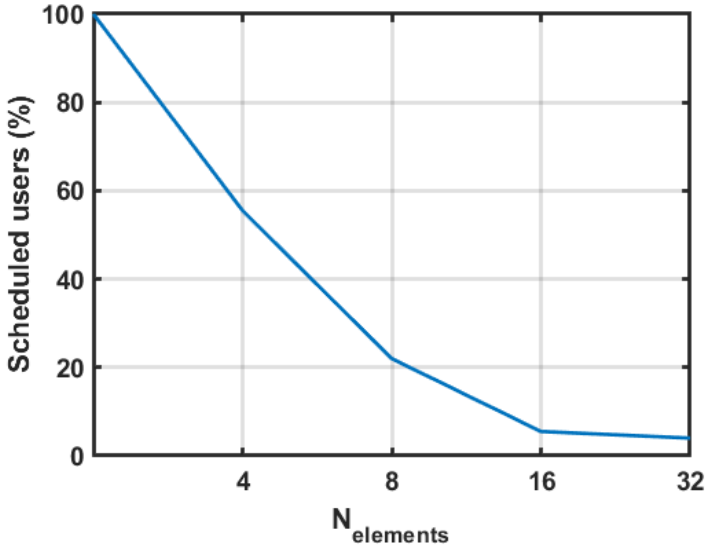

Figure 3.4: Amount of scheduled users over antenna elements, $\alpha = 0.5$.

3.2 User clustering for hybrid beamforming

In this section I extend my analysis to N_{RF} RF chains. Therefore I need to enhance the system model from the previous section. The received signal is now defined as

$$y_u = \sqrt{P_u}\mathbf{h}_u^{\mathsf{H}}\mathbf{P}_{RF}\mathbf{p}_{BB_u}\, x + n. \tag{12}$$

In addition to Eq. (4) it needs the baseband precoder $\mathbf{p}_{BBu} \in \mathbb{C}^{N_{RF}\times 1}$ for the user u, for combining the signals from each RF chain and now $\mathbf{P}_{RF} \in \mathbb{C}^{N_{elements}\times N_{RF}}$. The SNR calculation changes to

$$\mathrm{SNR}_u = \frac{\left\|\sqrt{P_u}\mathbf{h}_u^{\mathsf{H}}\mathbf{P}_{RF}\mathbf{p}_{BB_u}\right\|^2}{\sigma_n^2}. \tag{13}$$

3.2.1 Grouping

With multiple RF chains it is possible to form multiple beams, which makes it necessary to search for multiple groups of users, that can be served. For that purpose I adapted

a grouping algorithm from [21]. The original algorithm of the paper is supposed to search quasi orthogonal users, with reduced calculation effort. While it is important in a multi-user system to find orthogonal users, so they can be scheduled to the same resources, while minimizing the interference, in a single-user system with RF precoding the opposite is required, in order to have a matching precoder for grouped users. So I adapted the algorithm to search for similar users instead of orthogonal ones. The algorithm reads as follows:

- Step I: Initialize

$$\begin{aligned} \mathcal{S}_0 &= \mathbf{0} \\ \mathcal{T}_1 &= \{1, \ldots, |\mathcal{U}|\} \\ i &= 2 \end{aligned}$$

$$\begin{aligned} n &= \arg\max_{k \in \mathcal{T}_1} \|\mathbf{h}_k\|_2 \\ \mathbf{g}_1 &= \mathbf{h}_n \end{aligned}$$

$$\begin{aligned} \mathcal{S}_1 &= \mathcal{S}_1 \cup \{n\} \\ \mathcal{T}_i &= \{k \in \mathcal{T}_1 \neq n\} \end{aligned}$$

- Step II: For each user $k \in \mathcal{T}_i$ calculate

$$\mathbf{r}_k = \mathbf{h}_k \sum_{j=1}^{i-1} \frac{\mathbf{g}_j^{\mathsf{H}} \mathbf{g}_j}{\|\mathbf{g}_j\|_2^2}$$

- Step III: Select the ith user

$$\begin{aligned} n &= \arg\max_{k \in \mathcal{T}_i} \|\mathbf{r}_k\|_2 \\ \mathbf{g}_i &= \mathbf{h}_n \\ \mathcal{S}_1 &= \mathcal{S}_1 \bigcup \{n\} \\ \mathcal{T}_{i+1} &= \left\{ k \in \mathcal{T}_i \neq n \mid \frac{\left|\mathbf{h}_k \mathbf{g}_i^H\right|}{\|\mathbf{h}_k\|_2 \|\mathbf{g}_i\|_2} > \alpha \right\} \\ i &= i + 1 \end{aligned}$$

Go to Step II and repeat until $|\mathcal{S}_1| = M$, where M is the chosen group size or $\mathcal{T}_i$ is empty.

The algorithm is based on finding users with similar channel conditions, by projecting the channel of each user $\mathbf{h}_k$ to the space $\mathcal{G} = \text{span}\{\mathbf{g}_1, \ldots, \mathbf{g}_i\}$, where $\mathbf{g}_i$ is the channel vector from user n chosen in the ith iteration. Note that $\mathcal{G}$ is extended in every iteration. The algorithm starts with the user, which has the highest channel gain, and in every iteration the channel vector from the chosen user is added as a basis vector. At the end the users, which are considered in the next iteration are chosen with a threshold test.
The algorithm is repeated for every RF chain, resulting in N_{RF} orthogonal groups $\mathcal{S}_1, \ldots, \mathcal{S}_{N_{RF}}$ of M users each. All users that are getting scheduled are collected in

$$\mathcal{S} = \bigcup_{k=1}^{N_{RF}} \mathcal{S}_k, \tag{14}$$

where all users in $\mathcal{S}$ are getting scheduled uniformly distributed over all available resource blocks.

3.2.2 RF precoder

After the groups $\mathcal{S}_k$ of users are found, the RF precoder can be calculated as

$$\mathbf{h}_{RF_k} = \frac{\sum_{u \in \mathcal{S}_k} \mathbf{h}_u}{|\mathcal{S}_k|}, \tag{15}$$

$$\mathbf{P}_{RF} = \begin{pmatrix} \frac{\mathbf{h}_{RF_1}}{\|\mathbf{h}_{RF_1}\|} & \frac{\mathbf{h}_{RF_2}}{\|\mathbf{h}_{RF_2}\|} & \cdots & \frac{\mathbf{h}_{RF_{N_{RF}}}}{\|\mathbf{h}_{RF_{N_{RF}}}\|} \end{pmatrix} \tag{16}$$

This is analogous to the previous section the MRT for the averaged channel, repeated for every RF chain.

3.2.3 BB precoder

Last I can define the baseband precoder for user $u \in \mathcal{S}$, which I choose as simple selection precoder. Usually with this precoder, one aims for a technique that can suppress inter-user interference (IUI), but as I am still assuming a single-user scenario, where there is no IUI, this is not necessary. This precoder transmits the signal over the RF

chain, which has the highest effective channel gain. The effective channel for user u is defined as

$$\mathbf{h}_{eff_u} = \mathbf{P}_{RF}\mathbf{h}_u\sqrt{P_u}, \tag{17}$$

with $\mathbf{h}_{eff_u} \in \mathbb{C}^{1\times N_{RF}}$. With the effective channel the baseband precoder can then be defined as

$$i = \underset{l\in\{1,\dots,N_{RF}\}}{\arg\max} \left(|\mathbf{h}_{eff_u}\cdot\mathbf{e}_l|\right) \tag{18}$$

$$\mathbf{p}_{BB_u} = \mathbf{e}_i\,, \tag{19}$$

where $\mathbf{e}_i \in \mathbb{N}^{N_{RF}\times 1}$ is the ith unit vector, defined as

$$\mathbf{e}_1 = \begin{pmatrix}1\\0\\\vdots\\0\end{pmatrix}, \mathbf{e}_2 = \begin{pmatrix}0\\1\\\vdots\\0\end{pmatrix}, \dots, \mathbf{e}_{N_{RF}} = \begin{pmatrix}0\\0\\\vdots\\1\end{pmatrix} \tag{20}$$

In the normal case $i = k$ for $u \in \mathcal{S}_k$, because the RF precoder is calculated with the channels of the users in $\mathcal{S}_k$. In some cases it might happen that $i \neq k$ and the BB precoder regroups some users. This happens more often when the group size M is high and the threshold α is low, due to smaller correlation of the users channels.

3.2.4 Power constraint

With additional RF chains available it is important to talk about power constraints. In the system model the total transmit power stays the same independent of the set up, e.g. the number of RF chains or ULA elements. This refers to an overall power constraint. For the used SU system this constraint can be written as

$$\mathbb{E}_{x_u}\left\{\sum_{n=1}^{N_{RB}} P_{RB}\left\|\mathbf{P}_{RF}\mathbf{p}_{BB_u}x_u\right\|^2\right\} \leq P_{tx}\,, \tag{21}$$

where u is the user that is assigned to RB n. With the assumption that the transmit signal x_u has unit power $\mathbb{E}_{x_u}\left\{\|x_u\|^2\right\} = 1$, this equation can be equivalently expressed as

$$\sum_{n=1}^{N_{RB}} P_{RB}\left\|\mathbf{P}_{RF}\mathbf{p}_{BB_u}\right\|^2 \leq P_{tx} \tag{22}$$

Since the baseband precoder is defined as selection precoder $\mathbf{p}_{BB_u} = \mathbf{e}_i$, where i is the selected RF chain, Eq. (22) can be reduced to

$$\sum_{n=1}^{N_{RB}} P_{RB} \left\| \mathbf{P}_{RF_i} \right\|^2 \leq P_{tx} \,, \tag{23}$$

where $\mathbf{P}_{RF_i}$ is the ith column of $\mathbf{P}_{RF}$. Due to the equally distributed transmit power per RB $P_{RB} = \frac{P_{tx}}{N_{RB}}$ and $\|\mathbf{P}_{RF_i}\| = \|\frac{\mathbf{h}_{RF_i}}{\|\mathbf{h}_{RF_i}\|}\| = 1$ the overall power constraint is fulfilled.

3.2.5 Simulations

Similar to Sec. 3.1.1 I used a transmit power $P_{tx} = 40\,\mathrm{W}$ and the number of total users $|\mathcal{U}| = 200$. Again I am focusing on the behaviour of the beamforming and grouping technique, therefore the path loss $\xi_u = 110\,\mathrm{dB}$ is assumed for every user. The scheduling with the grouping algorithm is done in each time slot.

3.2.5.1 Grouping with equal group size M

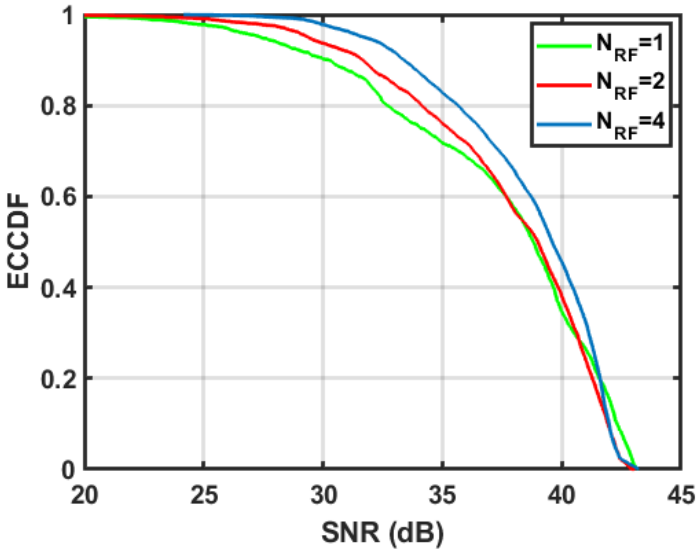

Figure 3.5: ECCDF of SNR for different numbers of RF chains, $M = 5$, $\alpha = 0.5$.

In Fig. 3.5 I show the ECCDF of SNR for different N_{RF}. With the group size M, the total amount of users getting scheduled is $M\,N_{RF}$. E.g for $N_{RF} = 4$ and $M = 5$, 20 users are getting scheduled in the same time slot. You can see that the SNR

for increasing N_{RF}, stays the same or increases slightly. This is the effect of the grouping algorithm, that is able to find multiple user groups with similar channel conditions. The slight increase of SNR for $N_{RF} = 4$, I interpret as diversity gain, because with more users scheduled, the chances are higher, that multiple users have good channel conditions. The performance of the grouping algorithm, and therefore the overall performance, is highly dependent on the parameters M and α. These are chosen, so that for the highest number of RF chains the algorithm is still able to find equally sized groups. With a too large group size or a too tight threshold, this might not be possible. Varying group sizes, leading to different amounts of users that are scheduled at the same time, may lead to high performance differences between the groups, which is related to the results made in Fig. 3.1 and 3.2. There the connection between the number of users and the achievable SNR was shown. With $M = 5$ and $\alpha = 0.5$ the goal of equal group sizes was achieved.
Fig. 3.6 shows the SNR of each individual group formed by the algorithm. All groups are performing almost the same, due to the chosen parameters.

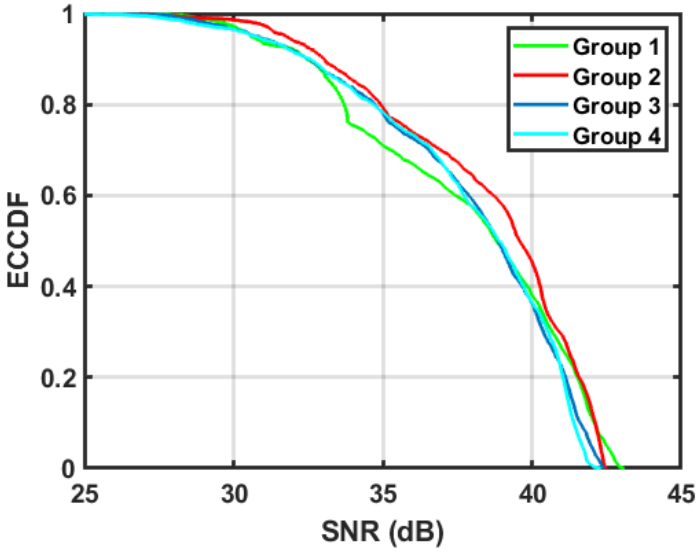

Figure 3.6: ECCDF of SNR for different groups,$M = 5$, $\alpha = 0.5$.

3.2.5.2 Grouping with varying group size M

Additionally I analysed the algorithm for varying group size M and a fixed amount of scheduled users $|\mathcal{S}| = 100$. Increasing the number of RF chains, leads then to a reduction in the group size. Because of this the group size can be very high for low numbers of N_{RF}. To make sure the algorithm is able to find these groups, I chose

$\alpha = 0$. The large group sizes and the small α might lead to a reassignment of the groups, when choosing the strongest RF chain with the BB precoder.

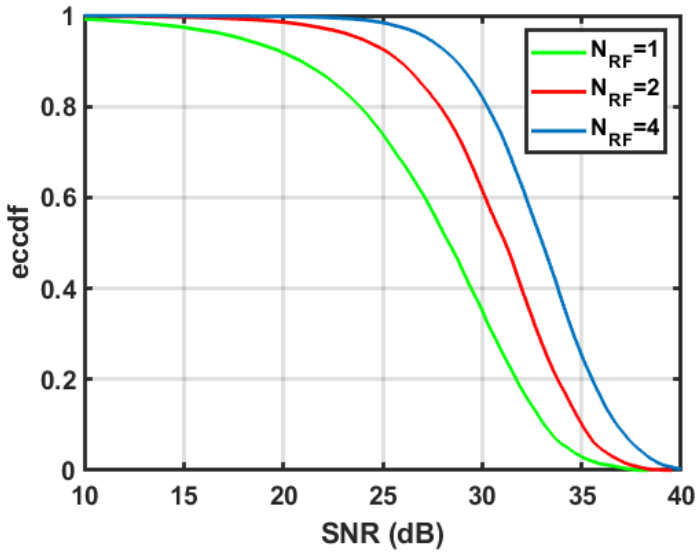

Figure 3.7: ECCDF of SNR for different numbers of RF chains, $M = \frac{|\mathcal{S}|}{N_{RF}}$, $\alpha = 0$.

In Fig. 3.7 I show the improvement of SNR, when increasing N_{RF}. The group size is reduced from 100 to 25, when N_{RF} increases from 1 to 4, leading to an overall SNR increase of $\sim 5\,$dB.

3.3 Distributed antenna system in a single-user scenario

In the last section of this chapter I extend the capability of my system model from one to multiple RAUs, where each RAU can be distributed in space. Note that each RAU is equipped with one ULA. The calculation of the received signal can be re-used from Eq. 12 with an additional sum for all RAUs, namely

$$y_u = \sum_{r=1}^{N_{RAU}} \sqrt{P_{u,r}} \mathbf{h}_{u,r}^H \mathbf{P}_{RF_r} \mathbf{p}_{BB_{u,r}} x + n \tag{24}$$

$$P_{u,r} = \xi_{u,r} P_{RB} \tag{25}$$

where $\mathbf{h}_{u,r}$ is the channel vector w.r.t. RAU r and equivalently $\mathbf{P}_{RF_r}$ and $\mathbf{p}_{BB_{u,r}}$ are the RF and baseband beamformer for RAU r. N_{RAU} is the number of RAUs. $P_{u,r}$ is the receive power w.r.t RAU r. Note that each RAU might have a different number of

RF chains N_{RF_r}. The SNR calculation changes to

$$\mathrm{SNR}_u = \frac{\left\| \sum_{r=1}^{N_{RAU}} \sqrt{P_{u,r}} \mathbf{h}_{u,r}^H \mathbf{P}_{RF_r} \mathbf{p}_{BB_{u,r}} \right\|^2}{\sigma_n^2}. \tag{26}$$

3.3.1 RF precoder

Now that the system model accounts for multiple transmit antennas, the RF precoding needs to be adapted. Until now all the users were split into N_{RF} groups and then the precoders where calculated according to these groups. With additional RAUs this is not directly possible, because each user has a different channel vector to each RAU. Therefore I choose to virtually assign the users to the RAU, for which the user has the smallest path loss. This may include shadowing and wall losses if considered. This procedure can be written as

$$r = \underset{\tilde{r} \in \{1,\ldots,N_{RAU}\}}{\arg\min} \; \xi_{u,\tilde{r}} \tag{27}$$

$$\mathcal{U}_r = \mathcal{U}_r \cup u \,, \tag{28}$$

where $\mathcal{U}_r$ is the group of users assigned to RAU r. With that the grouping algorithm defined in the previous section can be applied for each group $\mathcal{U}_r$ and for all RF chains to obtain the sets $\mathcal{S}_{r,k}$ of scheduled users on RAU r and RF chain k, resulting in $N_{RF_{tot}}$ groups, where $N_{RF_{tot}} = \sum_{r=1}^{N_{RAU}} N_{RF_r}$ is the total number of RF chains. The set of all scheduled users $\mathcal{S}$ is now defined as

$$\mathcal{S} = \bigcup_{r=1}^{N_{RAU}} \bigcup_{k=1}^{N_{RF_r}} \mathcal{S}_{r,k} \,. \tag{29}$$

The calculation of the RF precoder is then done with Eq. (15) and (16) , with the groups $\mathcal{S}_{r,k}$ for RAU r and RF chain k.

$$\mathbf{h}_{RF_{r,k}} = \frac{\sum_{u \in \mathcal{S}_{r,k}} \mathbf{h}_{u,r}}{|\mathcal{S}_k|}, \tag{30}$$

$$\mathbf{P}_{RF_r} = \left(\frac{\mathbf{h}_{RF_{r,1}}}{\left\|\mathbf{h}_{RF_{r,1}}\right\|} \quad \frac{\mathbf{h}_{RF_{r,2}}}{\left\|\mathbf{h}_{RF_{r,2}}\right\|} \quad \cdots \quad \frac{\mathbf{h}_{RF_{r,N_{RF_r}}}}{\left\|\mathbf{h}_{RF_{r,N_{RF_r}}}\right\|} \right) \tag{31}$$

3.3.2 BB precoder

The BB precoder is again chosen as selection precoder and can be calculated with the effective channel of each user u to each RAU r

$$\mathbf{h}_{eff_{u,r}} = \sqrt{P_{u,r}}\mathbf{h}_{u,r}^{H}\mathbf{P}_{RF_r} \,, \tag{32}$$

where $\mathbf{h}_{eff_{u,r}} \in \mathbb{C}^{1\times N_{RF,r}}$. To calculate the BB precoder the effective channel from all RAUs are stacked to one large vector

$$\mathbf{h}_{eff_u} = \begin{pmatrix}\mathbf{h}_{eff_{u,1}} & \mathbf{h}_{eff_{u,2}} & \dots & \mathbf{h}_{eff_{u,N_{RAU}}}\end{pmatrix}, \tag{33}$$

$\mathbf{h}_{eff_u} \in \mathbb{C}^{1\times N_{RF_{tot}}}$. After this, one can reuse Eq. (18) and (19), by changing N_{RF} to $N_{RF_{tot}}$ to get the BB precoding vector $\mathbf{p}_{BB_u} \in \mathbb{C}^{N_{RF_{tot}}\times 1}$. This leads to

$$\mathbf{p}_{BB_u} = \mathbf{e}_i \,, \tag{34}$$

where $\mathbf{e}_i$ is now the ith unit vector of length $N_{RF_{tot}}$. Since the BB precoding vector was calculated by stacking the effective channels of each RAU, $\mathbf{p}_{BB_u}$ is now split again into the corresponding vectors $\mathbf{p}_{BB_{u,r}}$ for each RAU r of size N_{RF_r} with

$$\mathbf{p}_{BB_u} = \begin{pmatrix}\mathbf{p}_{BB_{u,1}}\\ \mathbf{p}_{BB_{u,2}}\\ \vdots \\ \mathbf{p}_{BB_{u,N_{RAU}}}\end{pmatrix}. \tag{35}$$

This is needed to fit the model in Eq. (24).

3.3.3 Power constraint

In order to check the overall power constraint for the DAS, Eq. (22) changes to

$$\sum_{n=1}^{N_{RB}}\sum_{r=1}^{N_{RAU}} P_{RB}\left\|\mathbf{P}_{RF_r}\mathbf{p}_{BB_{u,r}}\right\|^2 \leq P_{tx}\,. \tag{36}$$

By using $\mathbf{p}_{BB_u}$ from Eq. (35) and

$$\mathbf{P}_{RF} = \begin{pmatrix}\mathbf{P}_{RF_1} & \mathbf{P}_{RF_2} & \dots & \mathbf{P}_{RF_{N_{RAU}}}\end{pmatrix}, \tag{37}$$

Eq. (36) can be written as

$$\sum_{n=1}^{N_{RB}} P_{RB}\left\|\mathbf{P}_{RF}\mathbf{p}_{BB_u}\right\|^2 \leq P_{tx}\,. \tag{38}$$

Since the BB precoder is still a selection precoder and chooses one RF chain from all available RF chains the overall power constraint is still fulfilled as discussed in Sec. 3.2.4. Note that the total transmit power P_{tx} is not increased by adding RAUs to the system.

3.3.4 Simulations

In my simulations I am comparing a scenario with one RAU and the same scenario with four distributed RAUs. For a realistic comparison I choose to use a 500x$500\,\mathrm{m}$ Manhattan building grid. This means that defined buildings and streets are placed in this area, simulating a city. The parameters are listed in Tab. 3.2.

Table 3.2: Manhattan grid parameters.

Building height	$25\,\mathrm{m}$
Building size	$50\,\mathrm{x}\,50\,\mathrm{m}$
Street width	$35\,\mathrm{m}$
BS antenna height	$32\,\mathrm{m}$
User antenna height	$2\,\mathrm{m}$
Wall loss	$20\,\mathrm{dB}$

The path loss model used is the urban macro (UMa) scenario from 3GPP TR 38.901 [22]. This model defines LOS and NLOS path loss and the simulator decides dependent on the LOS condition, defined by the geometry, which one is used. The geometry can be seen in Fig. 3.8. In both scenarios $|\mathcal{U}| = 100$ users where placed with the same randomly generated positions, to enable a fair comparison. The total transmit power of all RAUs $P_{tx} = 40\,\mathrm{W}$.

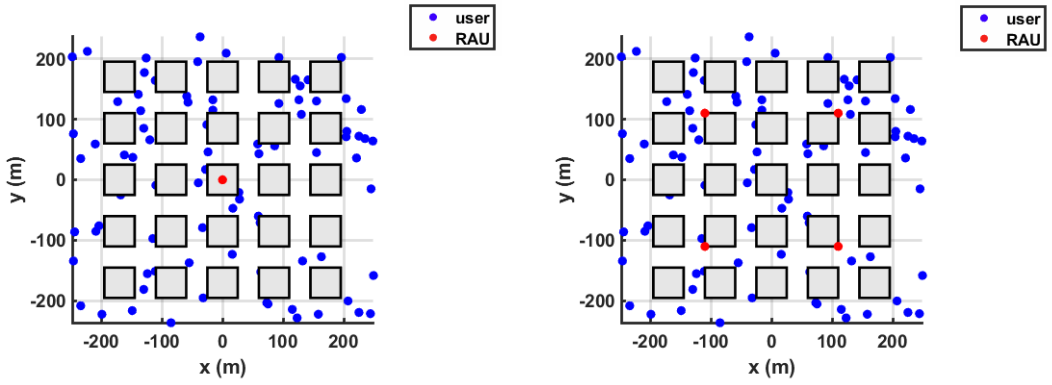

(a) Scenario 1 (b) Scenario 2

Figure 3.8: RAU and user placement for $N_{RAU} = 1$ and $N_{RAU} = 4$.

I used the grouping algorithm from Sec. 3.2 with varying group size dependent on the number of RF chains.

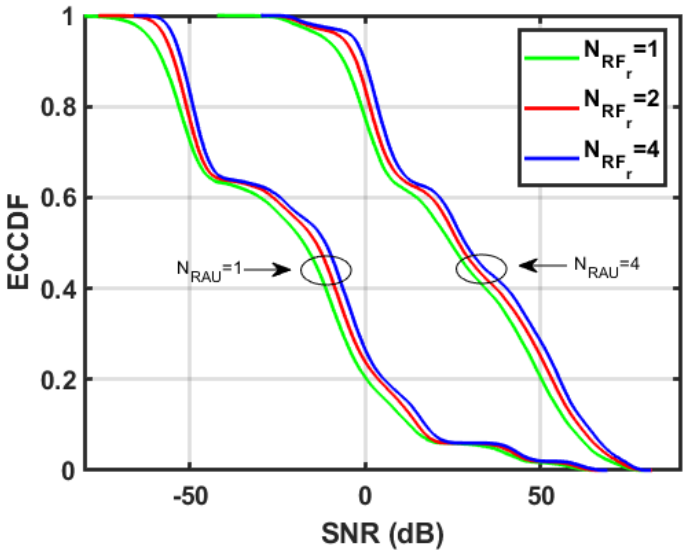

Figure 3.9: Comparison of a single RAU and four distributed RAUs with varying RF chains.

In Fig. 3.9 you can see the ECCDF of SNR for the different setups mentioned above. The cases $N_{RAU} = 1$ and $N_{RAU} = 4$ show the SNR for the scenario from Fig. 3.8a and Fig. 3.8b, respectively. For $N_{RAU} = 1$ the results behave similar to Fig. 3.7. The distribution of SNR is now associated with the used path loss model, but the performance is still increasing with higher number of RF chains, due to the smaller groups of users for each RF chain, resulting in better fitting beams. Looking at $N_{RAU} = 4$ you can see a major increase of SNR compared to scenario one. This is because many users are now served by a closer antenna and also have more likely a LOS connection. In other words you could decrease the transmit power by far for the same results, which is one important aspect of distributed antenna systems.

3.4 Conclusion

In this chapter I developed a single-user system, which is capable of hybrid precoding with multiple distributed RAUs. Within each section I showed simulation results to verify and analyse the performance of the components I used. The important aspects of this work were the behaviour of serving multiple users with one beam, the performance increase, when using multiple RF chains with a chosen grouping algorithm and at the end the increase of SNR, when using a DAS compared to a single transmit antenna. This is the basis, which was needed, for the multi-user system that I will introduce in the next chapter.

4 Multi-user analysis

In this chapter I introduce a multi-user system for DASs. The difference to a single-user system is that now a RB can be assign to multiple users. The advantage is that every RB that is re-used can increase the system capacity. However, it has the drawback that users assigned for the same RB interfere with each other, resulting in lower SINR. With the use of an interference cancellation strategy, this disadvantage can be eliminated. For that purpose AAs can make use of spatial multiplexing, which means that sharp spatial beams can be formed that do not interfere with each other. In case of hybrid BF the number of beams is limited to the number of RF chains, which also limits the number of users that can be assigned to the same RB. First I explain the system model and then I analyse the topics mentioned in Sec. 1.2, namely multiplexing, the impact of power constraints, channel estimation errors and scheduling. At the end of this chapter I compare the MU-DAS with a MU small cell system.

4.1 System model

In this section I describe the system model for a MU-DAS. The received signal for the user $u \in \mathcal{S}$ is defined as

$$y_u = \sum_{r=1}^{N_{RAU}} \sqrt{P_{u,r}} \mathbf{h}_{u,r}^{\mathsf{H}} \mathbf{P}_{RF_r} \mathbf{p}_{BB_{u,r}} x_u + \sum_{i \in \mathcal{S} \setminus u} \sum_{r=1}^{N_{RAU}} \sqrt{P_{i,r}} \mathbf{h}_{i,r}^{\mathsf{H}} \mathbf{P}_{RF_r} \mathbf{p}_{BB_{i,r}} x_i + n \quad (39)$$

$$P_{u,r} = \xi_{u,r} P_{RB} \quad (40)$$

As difference to the single-user system the transmit power per RB $P_{RB} = \frac{P_{tx}}{N_{RB}|\mathcal{S}|^2}$ is now divided additionally by $|\mathcal{S}|^2$, where $\mathcal{S}$ is the set of users, which got scheduled. This is necessary to sustain the overall transmit power P_{tx}, which will be explained in Sec. 4.1.3. Compared with Eq. (12) the second term in Eq. (39) is new and accounts for inter-user-interference. Therefore $\mathcal{S}$ also equals the users that share the same RBs and interfere with each other. The set $\mathcal{S}$ and the scheduling process is explained in more detail together with the precoder calculations and with an example. The SINR can now be defined as

$$\mathrm{SINR}_u = \frac{\left\| \sum_{r=1}^{N_{RAU}} \sqrt{P_{u,r}} \mathbf{h}_{u,r}^{\mathsf{H}} \mathbf{P}_{RF_r} \mathbf{p}_{BB_{u,r}} \right\|^2}{\sum_{i \in \mathcal{S} \setminus u} \left\| \sum_{r=1}^{N_{RAU}} \sqrt{P_{i,r}} \mathbf{h}_{i,r}^{\mathsf{H}} \mathbf{P}_{RF_r} \mathbf{p}_{BB_{i,r}} \right\|^2 + \sigma_n^2}. \quad (41)$$

4.1.1 RF precoder

The RF precoder is calculated similar to Sec. 3.3.1. The only thing that changes is the grouping algorithm. The adapted algorithm used in Sec. 3.2 was able to find users with

similar channel conditions, which was needed in a single-user system. In a multi-user system the original algorithm from [21] can be used to search quasi orthogonal users. This is necessary to reduce interference, as these users are getting scheduled to the same RBs. The output of the algorithm is the set $\mathcal{S}_r$ for each RAU, with

$$\mathcal{S} = \bigcup_{r=1}^{N_{RAU}} \mathcal{S}_r. \tag{42}$$

The size of $\mathcal{S}_r$ is $|\mathcal{S}_r| = N_{RF_r}$. This means that the algorithm searches one user for each RF chain in the system. With this each RF chain can form a beam with MRT for each user. The RF precoder is then defined as

$$\mathbf{P}_{RF_r} = \begin{pmatrix} \frac{\mathbf{h}_{\mathcal{S}_r(1)}}{\left\|\mathbf{h}_{\mathcal{S}_r(1)}\right\|} & \frac{\mathbf{h}_{\mathcal{S}_r(2)}}{\left\|\mathbf{h}_{\mathcal{S}_r(2)}\right\|} & \cdots & \frac{\mathbf{h}_{\mathcal{S}_r(N_{RF,r})}}{\left\|\mathbf{h}_{\mathcal{S}_r(N_{RF,r})}\right\|} \end{pmatrix}, \tag{43}$$

$$\mathbf{P}_{RF} = \begin{pmatrix} \mathbf{P}_{RF_1} & \mathbf{P}_{RF_2} & \cdots & \mathbf{P}_{RF_{N_{RAU}}} \end{pmatrix}. \tag{44}$$

This leads to one matched RF beam for each user and each user gets assigned the whole bandwidth or equivalently all RBs. The algorithm is repeated in every TS of the simulation. The size of $\mathcal{S}_r$ is discussed in more detail in the section below about the BB precoder.

4.1.2 BB precoder

With a limited number of users, it is generally only possible to find quasi orthogonal users that still interfere with each other to some extent. Also with the virtual assignment of the users to a RAU for the RF precoder calculation, it might happen that a beam from another RAU fits the wrong user generating significant interference. The goal is to cancel this interference with a properly chosen BB precoder. To achieve this goal the BB precoder needs to fulfill the following equation

$$\mathbf{h}_{eff_u}\mathbf{p}_{BB_i} \doteq 0,\ i \in \mathcal{S},\ i \neq u, \tag{45}$$

where $\mathbf{h}_{eff_u}$ is calculated with Eq. (32) and (33) using the RF precoder from Sec. 4.1.1. To solve this problem Eq. (45) can be written as

$$\mathbf{H}_{eff}\mathbf{P}_{BB} \doteq \mathbf{I}, \tag{46}$$

$$\mathbf{P}_{BB} = \begin{pmatrix} \mathbf{p}_{BB_1} & \mathbf{p}_{BB_2} & \cdots & \mathbf{p}_{BB_{|\mathcal{S}|}} \end{pmatrix}, \tag{47}$$

$$\mathbf{H}_{eff} = \begin{pmatrix} \mathbf{h}_{eff_1} \\ \mathbf{h}_{eff_2} \\ \vdots \\ \mathbf{h}_{eff_{|\mathcal{S}|}} \end{pmatrix}, \tag{48}$$

where $\mathbf{P}_{BB} \in \mathbb{C}^{N_{RF_{tot}} \times |\mathcal{S}|}$ is the baseband precoding matrix, $\mathbf{H}_{eff} \in \mathbb{C}^{|\mathcal{S}| \times N_{RF_{tot}}}$ is the effective channel matrix and $\mathbf{I}$ the identity matrix. The solution of Eq. (46) is then the Zero-Forcing (ZF) or null-steering precoder defined by the pseudo-inverse of the effective channel matrix

$$\mathbf{P}_{BB} = \mathbf{H}_{eff}{}^{\mathsf{H}} \left(\mathbf{H}_{eff} \mathbf{H}_{eff}{}^{\mathsf{H}} \right)^{-1}. \tag{49}$$

Note that the calculation of the pseudo-inverse of $\mathbf{H}_{eff}$ is only possible, when $\mathbf{H}_{eff}\mathbf{H}_{eff}{}^{\mathsf{H}}$ has full rank. The requisite for that is $N_{RF_{tot}} \geq |\mathcal{S}|$. As you can see here the RB re-use is bounded with the antenna configuration, if one aims for interference cancellation. To achieve the maximum performance in terms of frequency re-use I chose $|\mathcal{S}_r| = N_{RF_r}$, as already stated before. This leads to $|\mathcal{S}| = N_{RF_{tot}}$. This means that each RB gets re-used for every RF chain and every user is served by a matched beam, using the whole bandwidth. In general each user could have a different BB precoder for all RBs. However, as the channel during simulation is assumed to be flat Rayleigh fading, only one BB precoder is needed per user. The BB precoder $\mathbf{p}_{BB_u}$ for user u is then the uth column of $\mathbf{P}_{BB}$.

4.1.3 Power constraint

The overall power constraint for the MU-DAS can be formulated as

$$\mathbb{E}_{x_u} \left\{ \sum_{n=1}^{N_{RB}} \sum_{u \in \mathcal{S}} P_{RB} \left\| \mathbf{P}_{RF} \mathbf{p}_{BB_u} x_u \right\|^2 \right\} \leq P_{tx}\,. \tag{50}$$

Since I still assume unit power transmit signals the expectation and the transmit signal x_u can be dropped from the equation leading to

$$\sum_{n=1}^{N_{RB}} \sum_{u \in \mathcal{S}} P_{RB} \left\| \mathbf{P}_{RF} \mathbf{p}_{BB_u} \right\|^2 \leq P_{tx}\,. \tag{51}$$

This can be further simplified by using the BB precoding matrix instead of the sum over the vectors

$$\sum_{n=1}^{N_{RB}} P_{RB} \left\| \mathbf{P}_{RF} \mathbf{P}_{BB} \right\|^2 \leq P_{tx}\,. \tag{52}$$

Applying the Frobenuis norm $\|\cdot\|_F$ and using the Cauchy-Schwarz inequality Eq. (52) can be written as

$$\sum_{n=1}^{N_{RB}} P_{RB} \left\|\mathbf{P}_{RF}\right\|_F^2 \left\|\mathbf{P}_{BB}\right\|_F^2 \leq P_{tx} \,. \tag{53}$$

Note that $\left\|\mathbf{P}_{RF}\right\|_F^2 = N_{RF_{tot}}$, due to the definition of the RF precoder in Eq. (43) and (44). With the defined transmit power per RB $P_{RB} = \frac{P_{tx}}{N_{RB} {N_{RF_{tot}}}^2}$, the following needs to hold

$$\left\|\mathbf{P}_{BB}\right\|_F^2 \leq N_{RF_{tot}} \,, \tag{54}$$

to fulfill the overall power constraint. This is ensured by normalization of each column of $\mathbf{P}_{BB}$ with

$${\mathbf{P}_{BB}}^{norm} = \left(\frac{\mathbf{p}_{BB_1}}{\left\|\mathbf{p}_{BB_1}\right\|} \quad \frac{\mathbf{p}_{BB_2}}{\left\|\mathbf{p}_{BB_2}\right\|} \quad \cdots \quad \frac{\mathbf{p}_{BB_{|\mathcal{S}|}}}{\left\|\mathbf{p}_{BB_{|\mathcal{S}|}}\right\|} \right) , \tag{55}$$

which leads to

$$\left\|{\mathbf{P}_{BB}}^{norm}\right\|_F^2 = N_{RF_{tot}} \,, \tag{56}$$

Since the condition in Eq. (53) is based on the upper bound of the Chauchy-Schwarz inequality, this leads in general to a power loss. To avoid this the BB precoding matrix is scaled to

$$\left\|\mathbf{P}_{RF}\mathbf{P}_{BB}\right\|_F^2 = {N_{RF_{tot}}}^2 \,, \tag{57}$$

by

$${\mathbf{P}_{BB}}^{overall} = {\mathbf{P}_{BB}}^{norm} \frac{N_{RF_{tot}}}{\left\|\mathbf{P}_{RF}{\mathbf{P}_{BB}}^{norm}\right\|_F} \,. \tag{58}$$

This BB precoder fulfills the overall power constraint without any loss. Note that this normalization and scaling does not affect the condition in Eq. (45), still leading to interference cancellation. The BB precoding vector $\mathbf{p}_{BB_u}$ is then the uth column of ${\mathbf{P}_{BB}}^{overall}$, denoting the BB precoder that fulfills the overall power constraint without loss of power.

4.1.4 Scheduling

In this section the scheduling and how the set of scheduled users $\mathcal{S}$ is obtained are demonstrated with an example. I assume $N_{RAU} = 2$, $N_{RF_r} = 3$ and $|\mathcal{U}| = 50$. The first

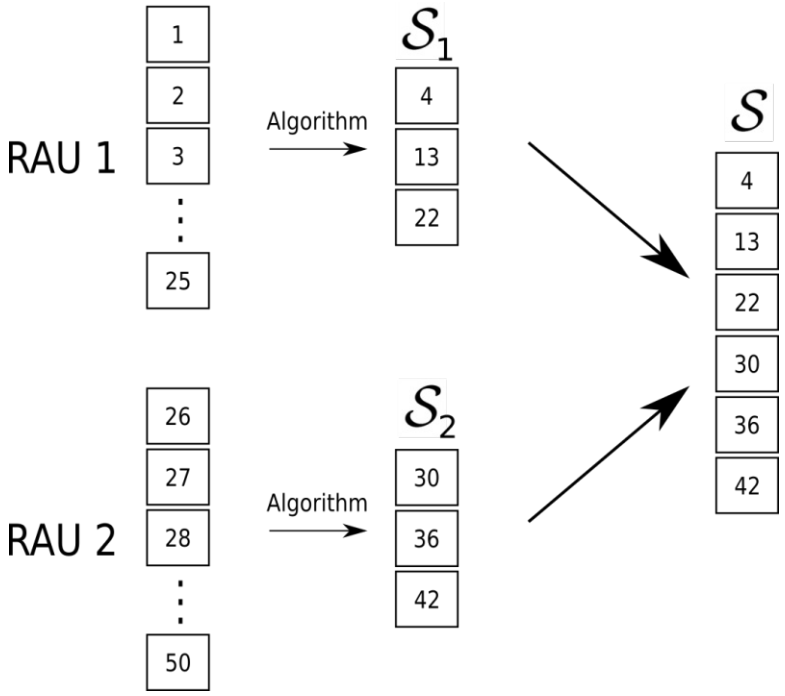

Figure 4.1: Scheduling example.

step is the assignment of the users to the RAUs, which was explained in Sec. 3.3.1. For example this could lead to 25 users for each RAU. After that the grouping algorithm searches one user for each RF chain. The grouping algorithm is done for each RAU separately. The found users are then collected in the sets $\mathcal{S}_r$ and $\mathcal{S}$. The procedure is illustrated in Fig. 4.1.
According to the resource grid of the simulator, each user in $\mathcal{S}$ then gets scheduled to all RBs. Fig. 4.2 shows a block diagram of the total hybrid precoding technique for this example. The explained scheduling is done in every time slot of the simulation and is referred as the default scheduling strategy.

4.1.5 Simulations

In this section I analyse the general behaviour of the introduced system, by varying different parameters. The fixed simulation parameters are listed in Tab. 4.1 and the used scenario is shown in Fig. 4.3.
First the difference between the selection and the ZF BB precoder is investigated. Fig. 4.4 shows the ECCDF of SINR for the selection BB precoder defined in Sec. 3.2 and the ZF BB precoder defined in Eq. (58). The SINR is up to 45 dB higher in the ZF case, because of the interference cancellation. Even though the grouping algorithm searches quasi orthogonal users, the generated interference without a proper BB precoder is

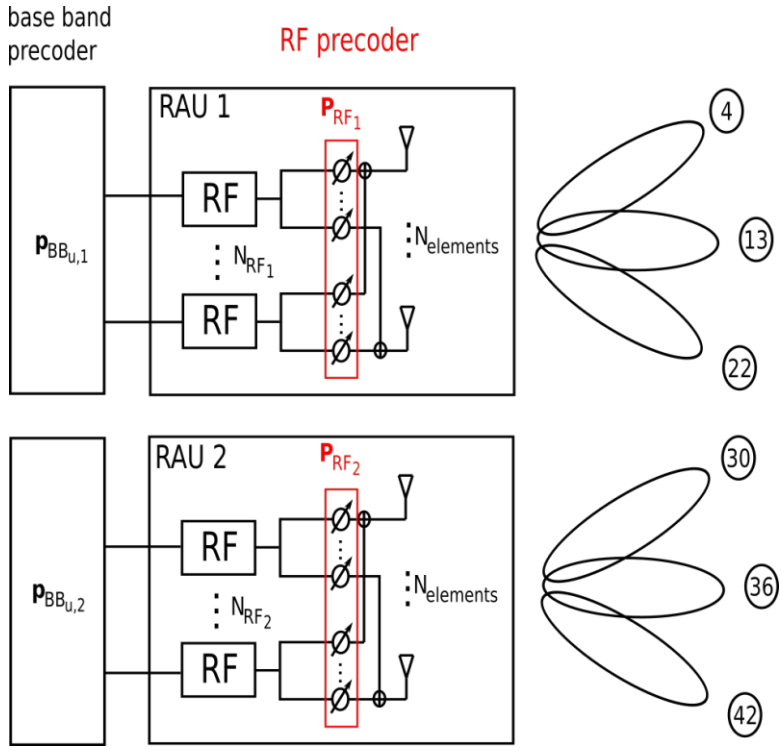

Figure 4.2: Hybrid precoding block diagram for the scheduling example, $N_{RAU} = 2$, $N_{RF_r} = 3$.

Table 4.1: Simulation parameters.

Carrier frequency	2 GHz
System bandwidth B	20 MHz
Subcarrier spacing	15 kHz
Number of resource blocks N_{RB}	100
Channel model	Rayleigh fading
Path loss model	TR 38.901 UMa
Transmit power	40 W
Users	100
N_{RAU}	4
Simulation time	1000 slots
Building height	25 m
Building size	50 x 50 m
Street width	35 m
BS antenna height	32 m
User antenna height	2 m
Wall loss	20 dB

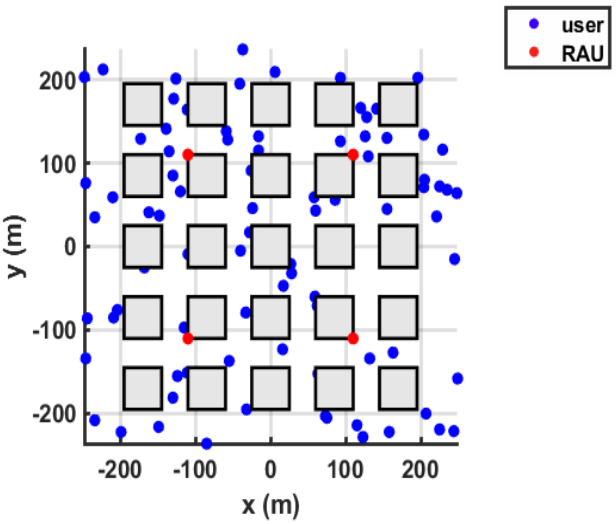

Figure 4.3: RAU and user placement, $N_{RAU} = 4$.

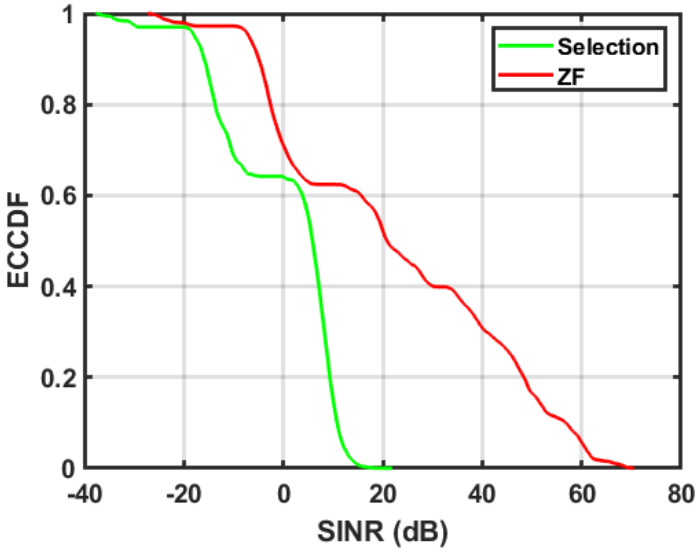

Figure 4.4: SINR of a Zero-Forcing and selection BB precoder, $N_{RF_r} = 4$, $N_{elements} = 16$.

significant. Have in mind that in this simulation setup 15 other users are scheduled to the same RBs, generating interference. The varying difference between these curves is explained by the LOS conditions of the users to the RAUs. Users with a LOS path to all RAUs suffer from far more interference then users with only one RAU in LOS. Note that these results are somewhat optimistic as I am only simulating one cell. In reality other cells would still generate interference and limit the achievable SINR, even though a DAS is used.
Now I analyse the general behaviour of the MU-DAS, when varying the number of RF chains and ULA elements. In all simulations the overall power constraint is met by using the BB precoding matrix $\mathbf{P}_{BB}{}^{overall}$ defined in Eq. (58). Fig. 4.5 shows the SINR for increasing number of RF chains N_{RF_r} per RAU. The SINR decreases with every RF

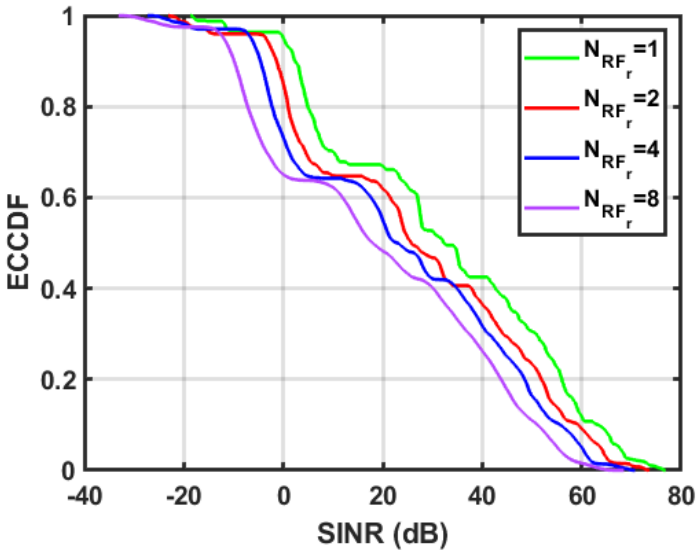

Figure 4.5: SINR for different numbers of RF chains, $N_{elements} = 16$.

chain, because this increases the number of parallel served users and the same transmit power is split between all of them. As explained in Sec. 4.1.3 this is necessary to fulfill the overall power constraint. On average this leads to a SINR decrease of $\sim 3\,\text{dB}$, when doubling N_{RF_r}.
In Fig. 4.6 the SINR for different ULA elements is shown. Due to the increasing beamforming gain the SINR increases for higher number of ULA elements.
Although the SINR per user decreases for increasing number of RF chains, as shown in Fig. 4.5, the higher frequency re-use can still increase the system capacity for every added RF chain. This can lead to higher total throughput, as long as each user has a good enough SINR. Fig. 4.7 shows the throughput for different numbers of RF chains and ULA elements.

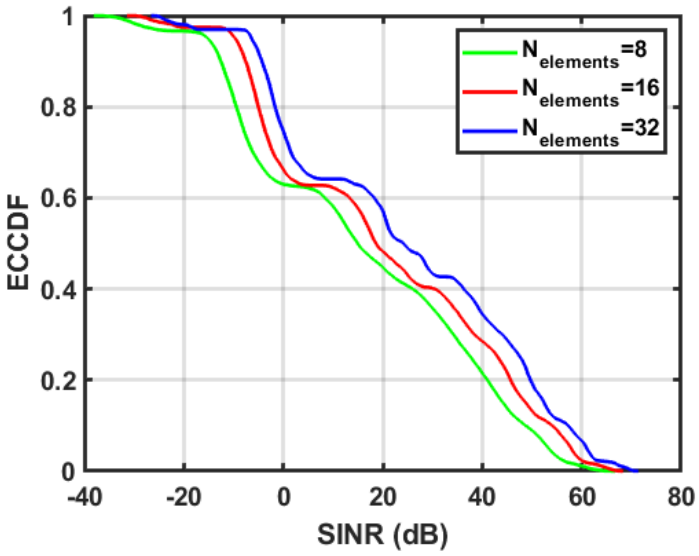

Figure 4.6: SINR for different ULA elements, $N_{RF_r} = 6$.

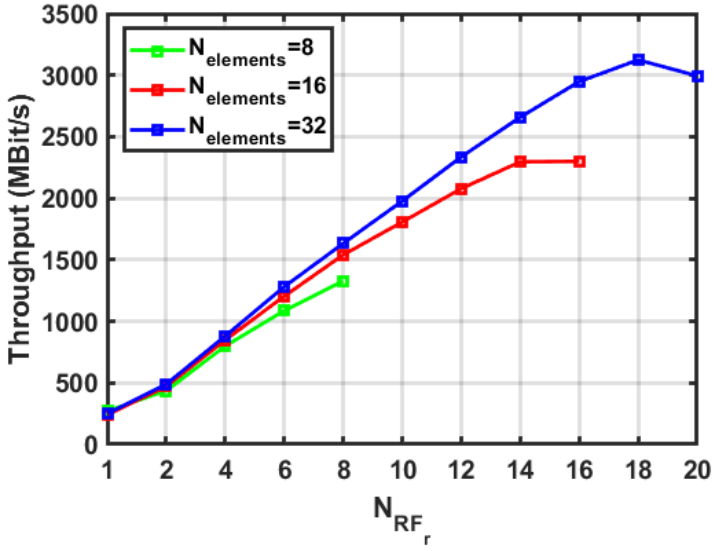

Figure 4.7: Throughput for different numbers of RF chains and ULA elements. [1]

[1]Note that there are only integer values of N_{RF_r} possible, but for better comparability lines are plotted between the points.

At low numbers of RF chains up to $N_{RF_r} = 4$ increasing the SINR by increasing the number of ULA elements has almost no impact on the achieved throughput. This indicates a saturation effect, which means the SINR is already high enough to provide the maximum data rates. When increasing the number of RF chains the throughput begins to flatten until a maximum is reached. After this point the throughput decreases even when the number of RF chains increase, which can be seen for $N_{elements} = 32$ and $N_{RF_r} = 20$. Here the SINR is too low to make effective use of the increased capacity in terms of total throughput. Note that the points $N_{RF_r} = 8$ and $N_{RF_r} = 16$ mark the limit of digital beamforming for $N_{elements} = 8$ and $N_{elements} = 16$, respectively, because then each ULA element can be connected to a RF chain.

4.2 Power constraints

Until now an overall power constraint was used, which splits the available power between all users and RBs uniformly. This was achieved by normalization of each column of the RF precoders $\mathbf{P}_{RF_r}$ and the BB precoder $\mathbf{P}_{BB}$. Although with this the total power is constrained, it is unknown which RF chain needs to carry how much power, before the calculation of the precoders is done. This can lead to problems, when dimensioning the power amplifiers for each RF chain. The problem here is that power amplifiers are only linear in a given regime. Without this knowledge, the amplifiers might cost even more, due to necessary overdimensioning. For that reason a power constraint that limits the power of each RF chain is more realistic. I refer to this as RF chain power constraint. With that said, most literature is still based on a per-RAU power constraint to limit the total system power [23][24]. In this section I compare the overall power constraint I used in the previous sections to the more realistic per-RF chain power constraint. Similar to the overall power constraint this can be achieved by correct normalization of the BB precoder. For simplicity I assume that the power of each RF chain is limited by $\frac{P_{tx}}{N_{RF_{tot}}}$. With this the power of every RF chain can be compared to the same reference, reducing computational complexity. Having a closer look on the dimensions of $\mathbf{P}_{BB}{}^{norm}$ defined in Eq. (55), one can see that the rows define the power of each RF chain and the columns define the power of each user. While normalization of the columns led to the overall power constraint, a simple normalization of the rows does not lead to the per-RF chain power constraint one would aim for. The reason for that is the condition in Eq. (45) would not hold anymore for interference cancellation, because the relations between the RF chains would get manipulated. This would introduce interference again. To achieve the per-RF chain power constraint, with perfect interference cancellation, one needs to scale the whole

BB precoder. This is done by searching the RF chain that carries the most power, with

$$Q_i = \sum_{u \in \mathcal{S}} \left| \mathbf{P}_{BB}{}^{norm}_{i,u} \right|^2 , \tag{59}$$

$$m = \max_{i \in (1 \ldots N_{RF_{tot}})} (Q_i) , \tag{60}$$

where $\mathbf{P}_{BB}{}^{norm}_{i,u}$ denotes the matrix element of the ith row and uth column of $\mathbf{P}_{BB}{}^{norm}$. Q_i stands then for the power that is carried by RF chain i. The new BB precoding matrix is then

$$\mathbf{P}_{BB}{}^{RF} = \mathbf{P}_{BB}{}^{norm} \frac{N_{RF_{tot}}}{\sqrt{m} \left\| \mathbf{P}_{RF} \mathbf{P}_{BB}{}^{norm} \right\|_F} . \tag{61}$$

The factor $\frac{N_{RF_{tot}}}{\left\| \mathbf{P}_{RF} \mathbf{P}_{BB}{}^{norm} \right\|_F}$ is again for the compensation of the losses, when using the Chauchy-Schwarz inequality. Note that now also the used total transmit power is reduced by the factor m, due to this down scaling of the BB precoder.

4.2.1 Simulations

In Fig. 4.8 the ECCDF of SINR for the overall and RF chain power constraint is shown for different numbers of RF chains per RAU N_{RF_r}. These simulations show that the per-RF chain constraint is overall more restrictive than the overall power constraint. While the difference between the two curves is only $\sim 0.9\,\text{dB}$ for $N_{RF_r} = 4$, it increases to $\sim 3.5\,\text{dB}$ for $N_{RF_r} = 12$.
This behaviour can be explained by the limitation of quasi orthogonal user channels in the scheduling, as well as the assignment of the users to the RAUs. Dependent on the match of each beam to a wrong user and the path loss to the respective RAU, the BB precoder assigns power to the RF chains. This results in a power distribution over the RF chains. Fig. 4.9 shows the power carried in each RF chain for user 7 in a sample slot, fulfilling the overall power constraint with $\mathbf{P}_{BB}{}^{norm}$. One would except a single peak at RF chain 7, since the RF precoder of this RF chain has been matched to user 7, but the figure shows that the calculation of the BB precoder leads to a power distribution between the RF chains. The distribution shows peaks at RF chain 7 and 29. This indicates that the beam formed by RF chain 29 fits quite well for user 7, which might happen because of the virtual assignment to the RAUs before the RF precoder calculation. The problem here is that with the assignment to a specific RAU the grouping algorithm cannot check if a beam also fits a user assigned to a different RAU.
If this effect happens to multiple RF chains, the power distribution can be in favor of a single RF chain. In this case RF chain 29 needs to carry triple the power of all others, which is shown in Fig. 4.10.

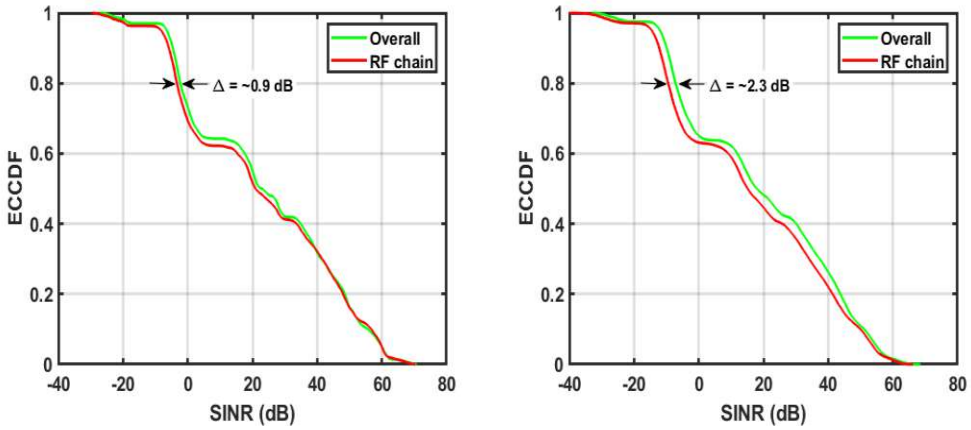

(a) $N_{RF_r} = 4$ (b) $N_{RF_r} = 8$

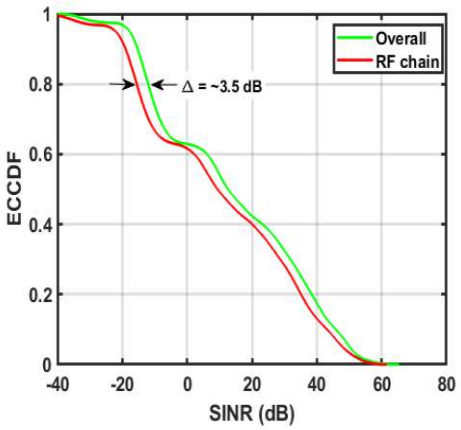

(c) $N_{RF_r} = 12$

Figure 4.8: Comparison of an overall and RF chain power constraint in terms of SINR, $N_{elements} = 16$.

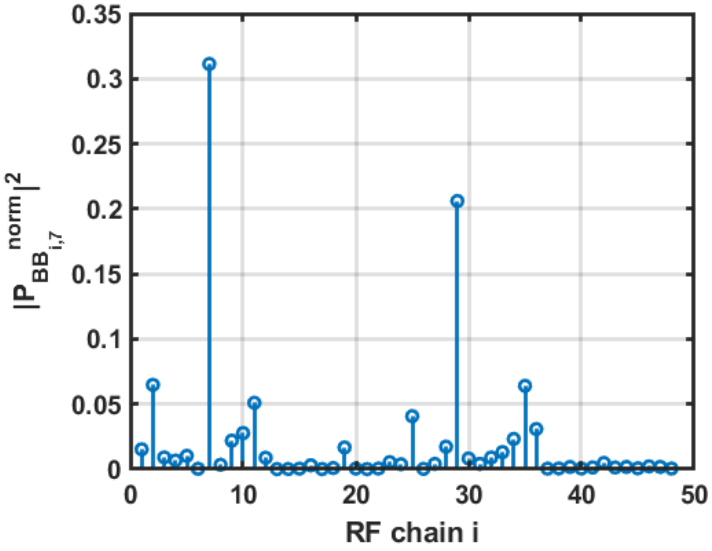

Figure 4.9: Power per RF chain for user 7, $N_{RF_r} = 12$.

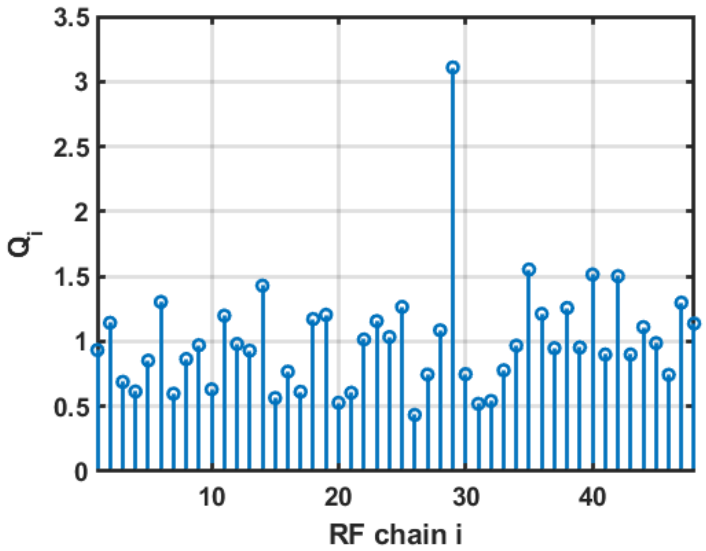

Figure 4.10: Total power distribution over RF chains, $N_{RF_r} = 12$.

As this effect is due to user channels that are not completely orthogonal, sharpening the beams, by increasing the number of ULA elements, improves this behaviour. Fig. 4.11 shows a comparison of the power constraints for $N_{elements} = 32$, reducing the difference from $\sim 3.5\,\text{dB}$ to $\sim 1.8\,\text{dB}$. The higher SINR is explained by the higher antenna gain for more ULA elements.

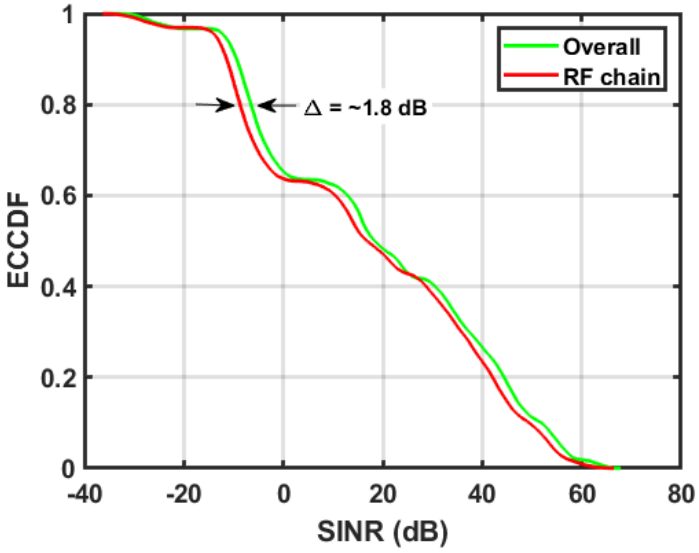

Figure 4.11: Comparison of an overall and RF chain power constraint for $N_{elements} = 32$, $N_{RF_r} = 12$.

Fig. 4.12 compares the total throughput of the overall and the RF chain power constraint. For low numbers of N_{RF_r} the difference between the constraints is hardly noticeable, while for higher numbers of N_{RF_r} applying the RF chain constraint lowers the throughput clearly.

4.3 Channel estimation errors

An important topic in state of the art cellular networks is channel estimation and the resulting channel estimation errors. In real systems the channel estimation is done with transmitted pilots that are known at the receiver. After estimating the channel at the receiver with these pilots a number of feedback bits is sent back to the base station that indicate a channel vector of a given codebook [25] [26]. This is necessary because the channel information must be known at the transmitter for the precoder calculations. The chosen codebook vector is typically found with a mean-square-error (MSE) criterion. This is done by comparing all codebook vectors with the estimated channel and choosing the one with the minimum mean-square-error (MMSE). In general a

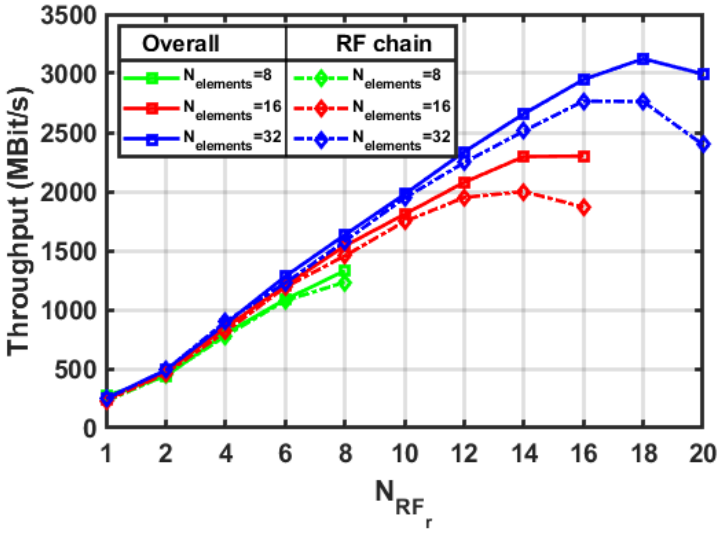

Figure 4.12: Throughput over RF chains and different ULA elements for an overall and RF chain power constraint.

larger codebook leads to reduced estimation error but needs more feedback bits in the transmission. As my system model does not consider a codebook based beamforming and the simulator is not capable of channel estimation I introduce an independent and identically distributed complex Gaussian channel estimation error $\mathbf{e}$ [27] [28]. The estimated channel $\tilde{\mathbf{h}}_{u,r}$ is then

$$\tilde{\mathbf{h}}_{u,r} = \mathbf{h}_{u,r} + \mathbf{e} \ , \ \ \mathbf{e} \in \mathbb{C}\mathcal{N}\left(0, \mathbf{I}_{N_{elements} \times N_{elements}} \sigma_e^2\right) \ , \tag{62}$$

where $\mathbf{I}$ is the identity matrix and σ_e^2 is the estimation error variance. $\mathbb{C}\mathcal{N}(\mu, \sigma^2)$ represents a complex Gaussian distribution with mean μ and variance σ^2. With this I can analyse the effect of channel estimation errors, by using the estimated channel for the precoder calculations and the real channel for the SINR calculation. In order to compare this channel estimation error with a realistic system, using a codebook, I estimate the number of feedback bits that would result in the given error variance σ_e^2, with the work of [29]. The authors in [29] stated that for users with full channel knowledge, where the channel estimation error results from the codebook design with the general Lloyd vector quantization [30], σ_e^2 can be estimated with rate-distortion theory. For Rayleigh fading this results in

$$\sigma_e^2 \simeq 2^{-\frac{B}{M}} \ , \ B \geq 0 \, , \tag{63}$$

where B is the number of feedback bits and M the length of a codebook vector. In my model $M = N_{elements}$. Reformulating Eq. (63) for B leads to

$$B \simeq -M \log_2(\sigma_e^2) \, , \, \sigma_e^2 \leq 1 \, . \tag{64}$$

4.3.1 Simulations

Fig. 4.13 shows SINR for different values of σ_e^2. The RF chain power constraint is applied for all simulations. It can be seen that the introduction of a channel estimation

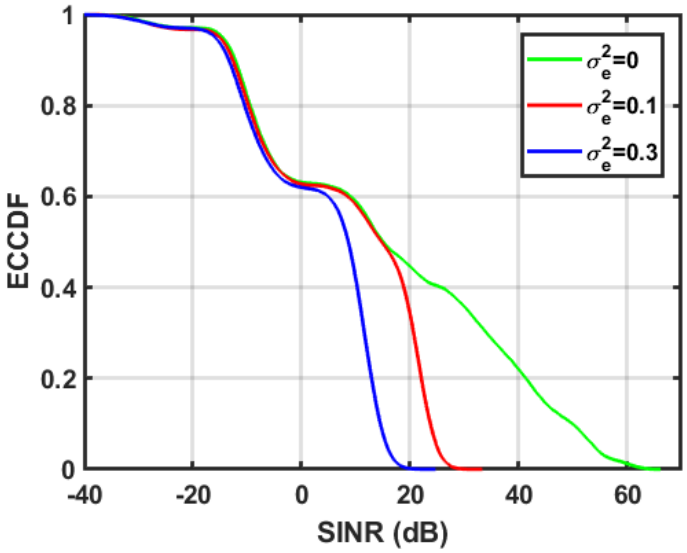

Figure 4.13: SINR for different σ_e^2, $N_{RF_r} = 8$.

error reduces the achievable SINR after reaching a breakpoint. Until this breakpoint all curves are almost the same, but after this point the SINR drops rapidly, with higher estimation erros having lower breakpoints. This indicates an upper bound of the SINR for a given estimation error. The reason for this is that the precoders do not match the actual channel, due to the estimation error, which leads to a ZF BB precoder that does not cancel the whole interference anymore. This means that for a large enough signal power the introduced interference limits the SINR to a upper bound. One could also say that the system switches at the breakpoint from a noise limited system to an interference limited system.
Increasing the total transmit power clearly demonstrates this upper bound, which is shown in Fig. 4.14. The increased transmit power provides $\sim 4.8\,$dB higher SINR in the low SINR regime. This matches the ratio of $10\log_{10}(\frac{120}{40})$. Beyond that the SINR reaches its limit and does not increase with transmit power anymore.

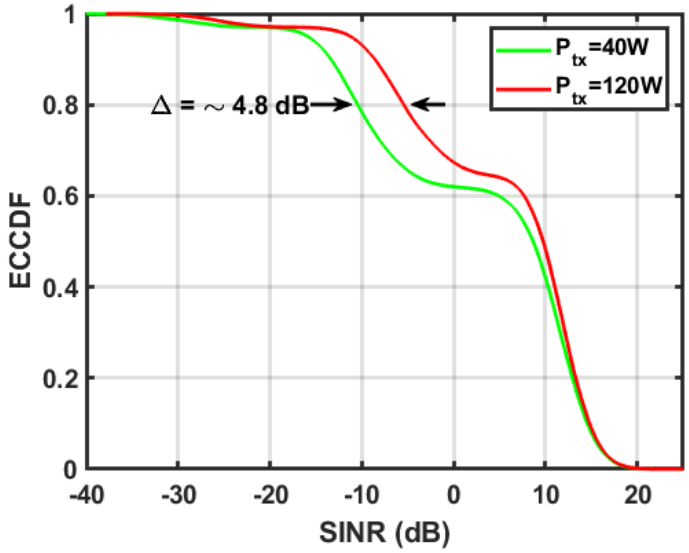

Figure 4.14: SINR for different transmit powers, $N_{RF_r} = 8$, $\sigma_e^2 = 0.3$.

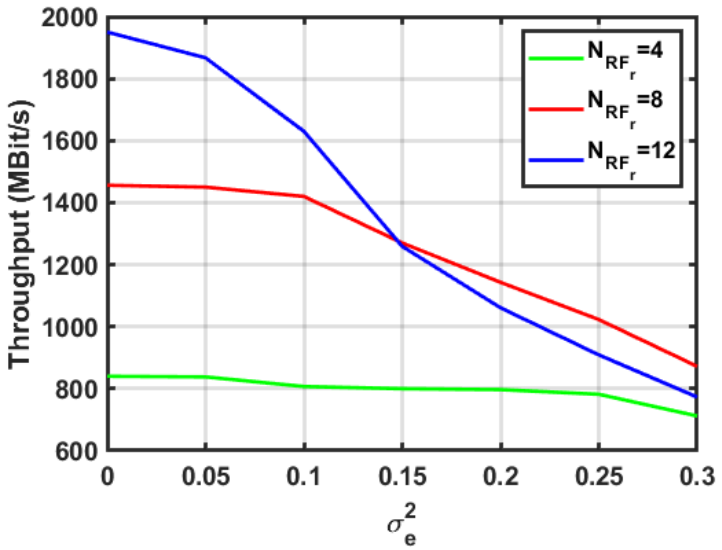

Figure 4.15: Throughput over σ_e^2 for different N_{RF_r}, $N_{elements} = 16$.

Fig. 4.15 shows the throughput over σ_e^2 for different numbers of RF chains. Due to the reduced SINR the throughput decreases with increasing error variance. While for $N_{RF_r} = 4$ the throughput decreases only slowly, it drops significant faster for $N_{RF_r} = 12$. The reason for that is the SINR saturation for $N_{RF_r} = 4$, explained in Sec. 4.1.5. Introducing the channel estimation error here will at first reduce this saturation before a decrease in throughput can be seen. With $N_{RF_r} = 12$ there is no saturation and the throughput decreases immediately.

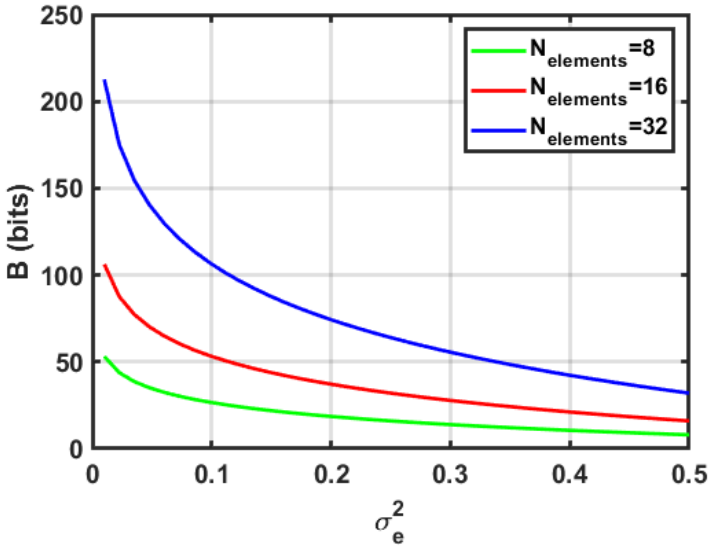

Figure 4.16: Feedback bits B for different ULA elements.

In Fig. 4.16 the number of needed feedback bits is shown, based on Eq. (64) for one RAU. As can be seen in Eq. (64) the number of feedback bits increases linearly with the number of ULA elements. As the figure shows the number of bits for a single RAU, one needs to multiply B by the number of RAUs, to get the total number of needed feedback bits $B_{tot} = N_{RAU}B$.

4.4 Scheduling

Besides increasing the data rates of 5G and beyond networks, providers also promise latency down to 1 ms or even below in the future. This is of particular importance for real time applications like autonomous driving or industry 4.0. Important factors for small latency are physical distance, the capability of the network distributing the data packets and the scheduling of the users. Whereas the first two points cannot be simulated with the 5G SLS, I analyse the aspect of scheduling and possible drawbacks. Scheduling in general determines, to which users data is transmitted at a given time.

This topic is important for minimizing latency, because the waiting time for a user could be to high even if the physical transmission and the network would allow a small latency. For example, when a user is scheduled every 40 ms, latency is limited to this 40ms, even though 20ms could be achieved physically.

4.4.1 Round robin scheduling

Until now the scheduling was purely based on a grouping algorithm from [21], which is a channel dependent scheduling strategy. As the channel realizations are random, the scheduling is random as well. This is not a solid approach in terms of fairness and latency. For that reason I consider a round robin (RR) scheduling strategy in this section. In order to do that I need to make sure that every user gets scheduled at least once in a given time. This is done with the following algorithm:

Step 1: User assignment to the RAUs according to the minimum path loss

$$r = \underset{\tilde{r}\in\{1,\dots,N_{RAU}\}}{\arg\min} \; \xi_{u,\tilde{r}} \tag{65}$$

$$\mathcal{U}_r^{(1)} = \mathcal{U}_r^{(1)} \cup u \,, \tag{66}$$

where $\mathcal{U}_r^{(1)}$ is the set of users assigned to RAU r for time slot $i = 1$.

Step 2: Apply the grouping algorithm to each set $\mathcal{U}_r^{(i)}$.

$$\mathcal{U}_r^{(i)} \rightarrow \mathcal{S}_r^{(i)} \,, \tag{67}$$

$$\mathcal{S}^{(i)} = \bigcup_{r=1}^{N_{RAU}} \mathcal{S}_r^{(i)} \,, \tag{68}$$

where $\mathcal{S}^{(i)}$ is the set of scheduled users in time slot i.

Step 3: Remove $\mathcal{S}_r$ from $\mathcal{U}_r^{(i)}$

$$\mathcal{U}_r^{(i+1)} = \mathcal{U}_r^{(i)} \setminus \mathcal{S}_r^{(i)} \tag{69}$$

$$i = i + 1 \tag{70}$$

Step 4: Repeat Step 2 and 3 for the following time slots i until $\mathcal{U}_r^{(i)} \leq N_{RF_r}$. The rest of the users in $\mathcal{U}_r^{(i)}$ get scheduled and all empty spots are filled with users that already got scheduled from $\mathcal{S}_r^{(1)}$. In the next time slot the algorithm starts again with $\mathcal{U}_r^{(1)}$.

In words the grouping algorithm is applied the usual way but the set of scheduled users $\mathcal{S}$ gets removed from the set of all users $\mathcal{U}$ for the next time slot. This is done until

each user was scheduled at least once and the process starts again with the full set of all users. With a fixed amount of users and RF chains in the scenario it can happen that at the end of the round robin process there are less users than RF chains. In general this is not a problem but RF chains that do not transmit any data would lead to a decrease in total throughput. For that reason I fill these spots with users that already got scheduled. The scheduling rate of user u is defined as

$$R_u = \frac{Number\ of\ schedules\ of\ user\ u}{Simulation\ time}\ . \tag{71}$$

Further the minimum scheduling rate among all users is defined as

$$R_{min} = \min_{u \in \mathcal{U}} (R_u)\ . \tag{72}$$

For the RR strategy R_{min} can be calculated with

$$R_{min}^{RR} = \frac{1}{\left\lceil \frac{|\mathcal{U}|}{\sum_{r=1}^{N_{RAU}} N_{RF_r}} \right\rceil}, \tag{73}$$

where $\lceil \cdot \rceil$ is the ceiling operator rounding up to the next integer. Fig. 4.17 shows the minimum scheduling rate for the RR scheduling strategy for different N_{RF_r}. Important

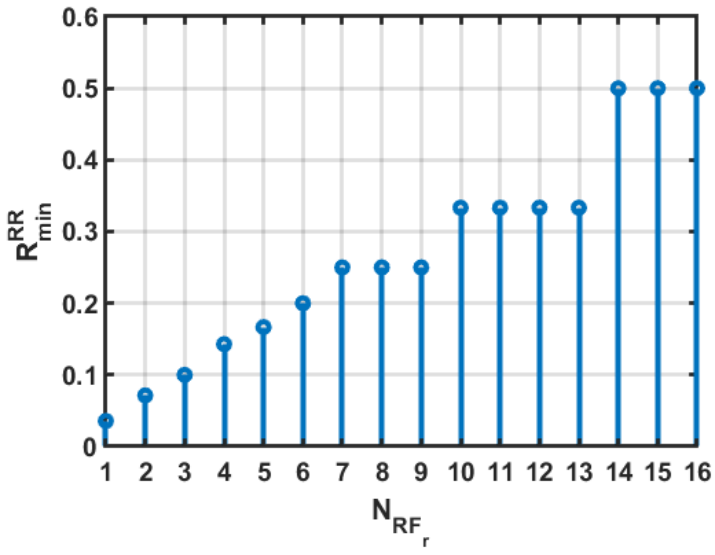

Figure 4.17: Minimum scheduling rate over number of RF chains for RR scheduling, $|\mathcal{U}| = 100$.

here is that R_{min}^{RR} does not increase with every RF chain. According to the scenario

and the chosen parameters it happens that R_{min}^{RR} stays constant for a given interval. This is because the RR algorithm guarantees that each user is at least scheduled every xth time slot, with $x = \left\lceil \frac{|\mathcal{U}|}{\sum_{r=1}^{N_{RAU}} N_{RF_r}} \right\rceil \; x \in \mathbb{N}$. Note that this only makes sense when x is a integer. Therefore R_{min}^{RR} only increases when x reaches the next integer value. In that sense, the default scheduling strategy explained in Sec. 4.1.4 can not guarantee a certain scheduling rate at all, because the scheduling is only done according to the random channel. On average the scheduling rate will increase with higher numbers of RF chains, but will vary dependent on the channel characteristics and cannot be guaranteed in a certain time interval.

4.4.1.1 Simulations

Fig. 4.18 shows the SINR for the default and the RR scheduling strategy. It can be seen that the SINR is lower for the RR strategy and the difference to the default strategy increases with the number of RF chains. The reason for this is that the grouping algorithm is not performing as intended anymore. The problem is that in every time slot the number of users to choose from gets smaller. This makes it necessary to schedule just the users that are available, independent of their channel conditions. Therefore users with bad channel conditions get scheduled, reducing the SINR. The more users getting scheduled with bad channel conditions the higher is the loss in SINR, this explains the increasing difference to the default scheduling strategy for higher numbers of RF chains.

4.4.2 Extended user scheduling

Up to this point only one user got scheduled per RF chain, which achieves the maximum BF gain, but limits the number of scheduled users to the number of RF chains. Another way to increase the scheduling rate would be to schedule more users per RF chain. For that I use the RR algorithm from Sec. 4.4.1 as basis and extend it by applying the grouping algorithm K times. As now more users are served by the same RF beam the RF precoder is now calculated with the averaged channel of those users, similar to Sec. 3.3.1. To recap the RF precoder is now defined as

$$\mathbf{h}_{RF_{r,k}} = \frac{\sum\limits_{u \in \mathcal{S}_{r,k}} \mathbf{h}_{u,r}}{|\mathcal{S}_k|}, \tag{74}$$

$$\mathbf{P}_{RF_r} = \begin{pmatrix} \frac{\mathbf{h}_{RF_{r,1}}}{\left\|\mathbf{h}_{RF_{r,1}}\right\|} & \frac{\mathbf{h}_{RF_{r,2}}}{\left\|\mathbf{h}_{RF_{r,2}}\right\|} & \cdots & \frac{\mathbf{h}_{RF_{r,N_{RF,r}}}}{\left\|\mathbf{h}_{RF_{r,N_{RF,r}}}\right\|} \end{pmatrix}. \tag{75}$$

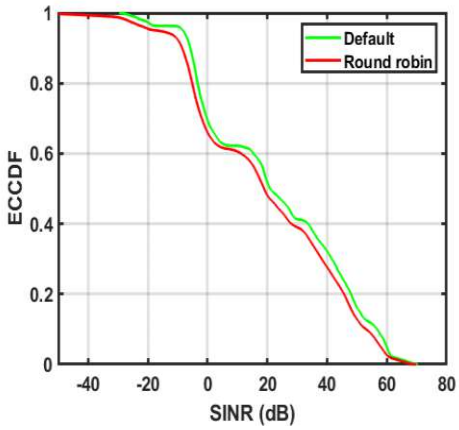

(a) $N_{RF_r} = 4$

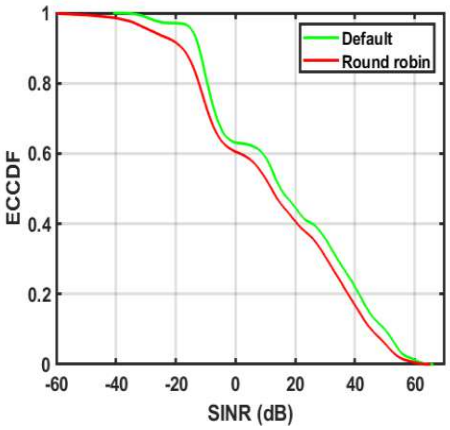

(b) $N_{RF_r} = 8$

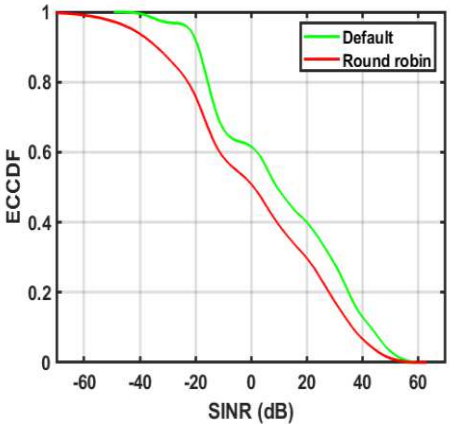

(c) $N_{RF_r} = 12$

Figure 4.18: Comparison of the default and round robin scheduling in terms of SINR, $N_{elements} = 16$.

The set $\mathcal{S}_{r,k}$ is then the set of scheduled users for RAU r and RF chain k, with $|\mathcal{S}_{r,k}| = K$. The minimum scheduling rate can now be calculated with

$$R_{min}^{RR} = \frac{1}{\left\lceil \frac{|\mathcal{U}|}{K \sum_{r=1}^{N_{RAU}} N_{RF_r}} \right\rceil}. \tag{76}$$

Note that $K = 1$ leads to the same results as in Sec. 4.4.1. Fig. 4.19 shows the minimum scheduling rate defined in Eq. (76) for different K. It shows that the minimum

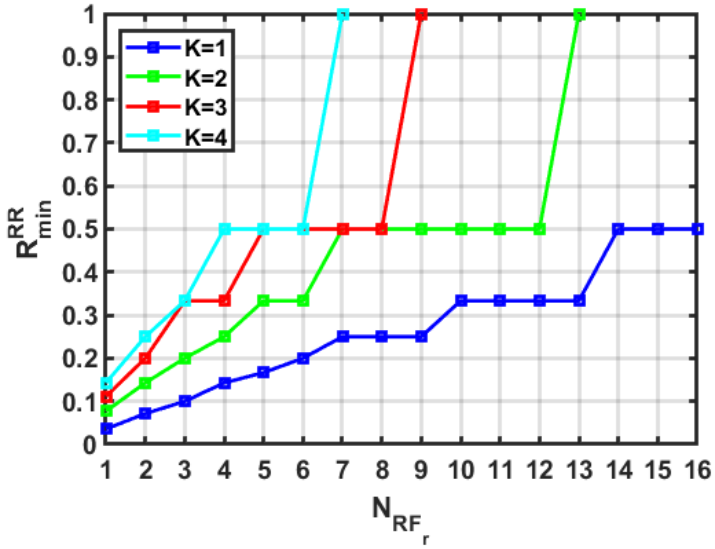

Figure 4.19: Minimum scheduling rate for different K, $N_{elements} = 16$.

scheduling rate can be scaled drastically, when increasing K. For example with $K = 2$ only seven RF chains per RAU are required to guarantee a minimum scheduling rate of $50\,\%$, while for $K = 1$, 14 RF chains would be needed. Also it is only possible to achieve a minimum scheduling rate of $100\,\%$, when $K > 1$, which means that each user gets scheduled in every time slot.

4.4.2.1 Simulations

In Fig. 4.20 the SINR for different values of K is shown. Even though the scheduling rate increases with K the SINR decreases. This happens because now one RF beam needs to serve multiple users. In an optimal system, the users scheduled for the same RF chain would have fully correlated channels while still being orthogonal to all other users. As the number of users is limited this is not possible and the channels of the users scheduled for the same RF chain will not be fully correlated. This reduces the

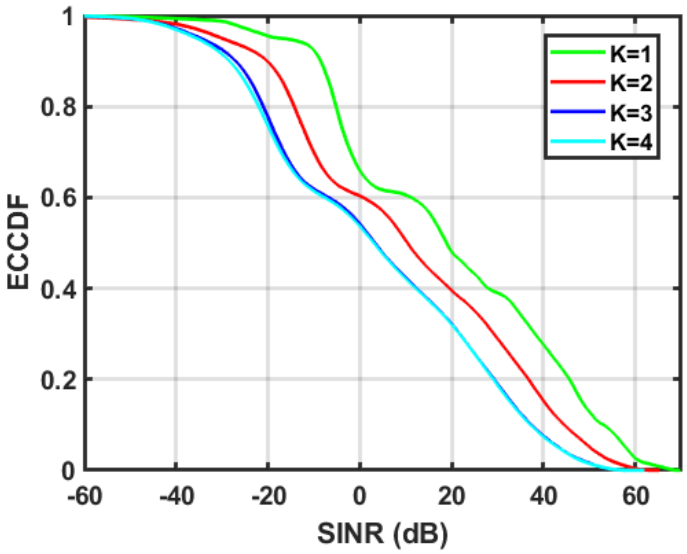

Figure 4.20: SINR for different K, $N_{RF_r} = 4$, $N_{elements} = 16$.

beamforming gain from the RF precoder, due to the calculation with the averaged channel. When too many users are scheduled for one RF chain, that are not correlated, the RF precoder starts to act as a random beamformer for the individual users. This explains the matching SINR for $K = 3$ and $K = 4$. This shows that high scheduling rates might come only at the high cost of reduced SINR and total throughput.

4.5 Comparison of DAS and small cell structures

In this section I compare a DAS with a small cell structure. For that I use the four RAUs in Fig. 4.3 as base stations of stand alone small cells. Both systems have the same goal of providing better coverage and higher capacity. While the DAS achieves this goal by deploying multiple RAUs in the cell, the small cell system increases the number of cells. These strategies differ in many points. First of all each user can be served by all RAUs simultaneously in the DAS, while in the small cell system each user is only served by one of them. This increases the computational effort for the DAS, because one base station needs to do the signal processing for all RAUs. For example the channel estimation needs to be done for all RAUs in the DAS. This also increases the data traffic from the users to the base station. In general the DAS has higher total costs according to [31]. Keeping in mind that mobile users are moving, the network needs to do a handover, whenever a user crosses a cell edge. This will happen more frequently in a small cell system. Also the requirements on the connection to the wired core network, called the backhaul, are different for small cells and DASs. In the small cell system every cell requires its own backhaul connection to the core,

whereas the DAS requires only one backhaul connection. A specific difference in terms of beamforming would be that small cells can only cancel the inter-beam interference from their own base station, while in a DAS the inter-beam interference from all RAUs is cancelled. However, this requires coherent signal detection at the user, which can be a difficult task dependent on the wireless propagation environment.

4.5.1 Simulations

In my simulations I use a total transmit power $P_{tx} = 40\,\mathrm{W}$ for both systems. In the small cell system the transmit power is equally distributed between the cells. For a fair comparison the small cells and the DAS have the same total number of RF chains and the RF chain power constraint is applied. To achieve the best performance in terms of SINR and throughput I use the default scheduling strategy. For variation in the scenario I simulate the systems with and without the Manhattan building grid. This provides a scenario with pure LOS and one with mixed LOS/NLOS conditions.

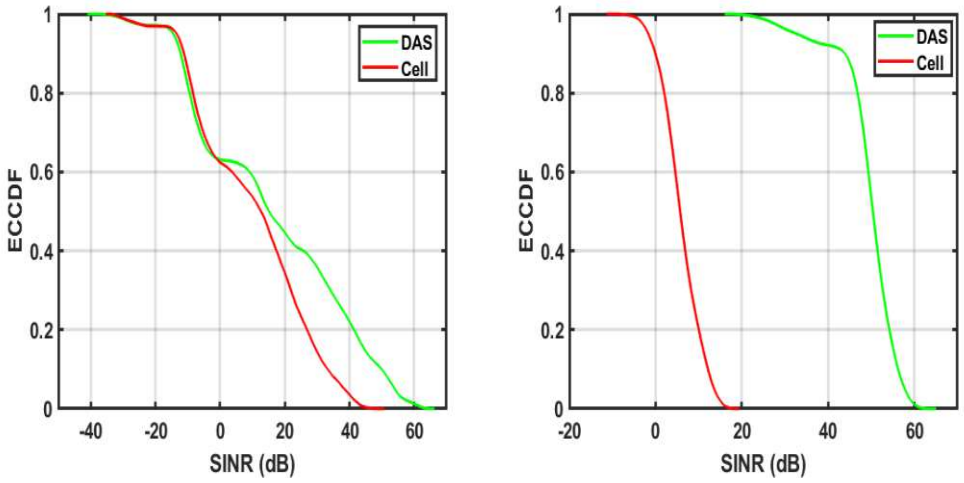

(a) Manhattan building grid scenario (b) Pure LOS scenario

Figure 4.21: SINR for DAS and small cell system for Manhattan building grid and pure LOS scenario, $N_{RF_r} = 8$, $N_{elements} = 16$.

Fig. 4.21a and b show the SINR of both systems in the Manhattan building grid and the pure LOS scenario. In Fig. 4.21a in the low SINR regime both systems perform close to each other, while at higher SINR the introduced inter-cell interference reduces the SINR of the small cell system. These two different behaviours can be explained by the LOS conditions of the users to the base stations. When in a small cell system only one base station is in LOS to the user, it can achieve the same SINR, but if multiple base stations are in LOS the additional interference reduces the SINR of the small cell

system. When removing the Manhattan building grid in Fig. 4.21b from the scenario the two systems react in opposite directions. While the SINR increases significantly in the DAS, it decreases in the small cell system. The reason for that is the pure LOS environment that increases the signal strength. For the DAS, where all interference is cancelled, this results in an increased SINR. The small cell system suffers from severe inter-cell interference from the base stations that are now in LOS to the users.
Note that these results are rather optimistic, because out-of-cell interference from other base stations will always limit the achievable SINR, which I do not simulate. Especially in the pure LOS scenario the SINR of the DAS would suffer from this out-of-cell interference.
In Fig. 4.22 the comparison of the throughput is shown. The solid lines represent the Manhattan building scenario and the dash-dotted lines the pure LOS scenario. In the Manhattan building grid scenario the small cell system has 200 MBit/s lower throughput at $N_{RF_r} = 12$, due to the lower SINR. In the pure LOS scenario the small cell system reaches its limits at 900 MBit/s, while the throughput for the DAS increases almost linearly with RF chains.

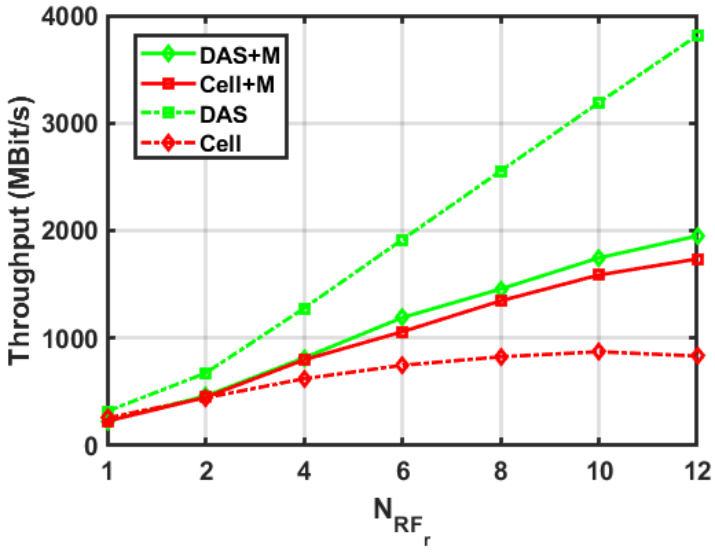

Figure 4.22: Throughput for DAS and cell structure with and without Manhattan building grid.

At the end I have a look on the power constraints, when using the small cell system. Fig. 4.23 shows the difference between the overall and RF chain power constraint for $N_{RF_r} = 8$ in the pure LOS scenario.
Comparing Fig. 4.23a and b the RF chain power constraint is not more restrictive than the overall power constraint in the small cell system. For the DAS the difference

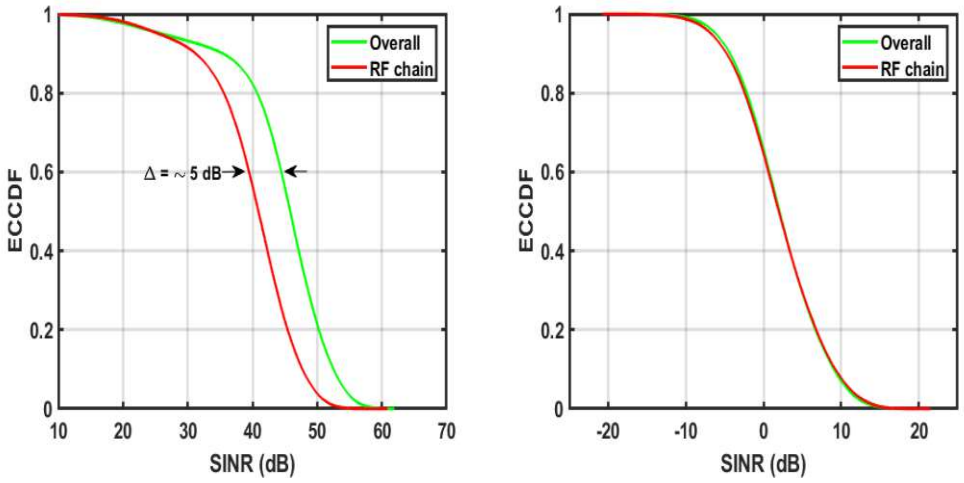

(a) DAS (b) Small cells

Figure 4.23: SINR for overall and RF chain power constraint in a pure LOS scenario, $N_{RF_r} = 12$.

between the constraints is $\sim 5\,\text{dB}$. As explained in Sec. 4.2.1 the problem are RF beams from other RAUs that match not intended users. This favors single RF chains to carry more power, which leads then to a total power reduction in order to fulfill the RF chain power constraint. In the pure LOS scenario theses matching RF beams are also in LOS, resulting in a higher difference to the overall power constraint than in the Manhattan building grid scenario shown in Fig. 4.8c. As the small cell system does not consider RF beams from other base stations in the precoder calculation it does not have this problem.

5 Conclusion

This thesis has shown multiple results regarding DAS. First basic analysis of hybrid beamforming was done, showing the trade-off between the number of users that are served by the same RF beam and the achievable SNR. The usage of more RF chains and a suited grouping algorithm can increase the number of scheduled users without reducing the SNR, or the same number of users can be split in smaller groups increasing the SNR.
Then the system was extended to a multi-user system. The investigation and comparison of two power constraints has shown that a per RF chain power constraint is more restrictive than an overall power constraint in a DAS. Simulations have then shown that this is not the case for a small cell system. The reason for this was the assignment of the users to the RAUs before the grouping algorithm for scheduling and precoder calculation could be applied. To avoid this, the user assignment should be dropped and a grouping algorithm that uses the channels of all users to all RAUs should be considered.
The introduction of channel estimation errors has shown that imperfect channel knowledge will lead to a upper bound of SINR. As channel estimation errors are always done when sending the channel information from the user to the base station, a high enough number of feedback bits needs to be transmitted to indicate the channel vector of a codebook. In a DAS the channel estimation has to be done for all RAUs. At a certain number of RAUs this might lead to complexity issues, because the users need to estimate all channels and the feedback bits need to be sent for each RAU.
As channel based scheduling is random by nature it is not suited for providing a guaranteed scheduling rate, which is required when considering latency requirements. Combining the channel based scheduling with a round robin strategy and scheduling additional users per RF chain has shown that there is a substantial trade-off between the achievable SINR and high scheduling rates.
At the end of the thesis a DAS was compared to a small cell system in a Manhattan building grid and a free space scenario. The results indicate that as soon as multiple RAUs have a LOS connection to users, the DAS performs better than the small cell system, because the users suffer from higher interference in the small cell system.

5.1 Improvements

In this section possible improvements of the introduced system are mentioned.

An important aspect, which was not considered, is out-of-cell interference. Even with a DAS other cells will generate interference. Simulating multiple cells of a DAS or a DAS surrounded by small cells will provide more realistic results. A special problem could be the generated interference at cell edges.

A second improvement would be the usage of a grouping algorithm, that substitutes the user assignment to the RAUs. As mentioned in the conclusion this could improve the performance when considering a per RF chain power constraint. Also important would be how the complexity scales using such algorithms when the number of RAUs increases.

Another improvement would be a flexible power distribution to the users, dependent on path loss and LOS condition. In many of the results some users have a SINR at such a high level, where there is not much profit anymore. Using more power for users that have bad propagation conditions could improve overall performance and fairness.

6 References

[1] A. Alexiou, P. Demestichas, and A. Georgakopoulos, "5G vision, enablers and challenges for the wireless future," *Wireless Res. Forum, White Paper*, 2015.

[2] Qualcomm. (2013, Nov.) The 1000x mobile data challenge. https://www.qualcomm.com/documents/1000x-mobile-data-challenge.

[3] A. Alkhateeb, J. Mo, N. Gonzalez-Prelcic, and R. W. Heath, "MIMO precoding and combining solutions for millimeter-wave systems," *IEEE Communications Magazine*, vol. 52, no. 12, pp. 122–131, 2014.

[4] T. S. Rappaport, S. Sun, R. Mayzus, H. Zhao, Y. Azar, K. Wang, G. N. Wong, J. K. Schulz, M. Samimi, and F. Gutierrez, "Millimeter wave mobile communications for 5G cellular: It will work!" *IEEE Access*, vol. 1, pp. 335–349, 2013.

[5] S. Rangan, T. S. Rappaport, and E. Erkip, "Millimeter-wave cellular wireless networks: Potentials and challenges," *Proceedings of the IEEE*, vol. 102, no. 3, pp. 366–385, 2014.

[6] M. J. Crisp, S. Li, A. Wonfor, R. V. Penty, and I. H. White, "Demonstration of a radio over fibre distributed antenna network for combined in-building WLAN and 3G coverage," in *OFC/NFOEC 2007 - 2007 Conference on Optical Fiber Communication and the National Fiber Optic Engineers Conference*, 2007, pp. 1–3.

[7] M. K. Müller, F. Ademaj, T. Dittrich, A. Fastenbauer, B. R. Elbal, A. Nabavi, L. Nagel, S. Schwarz, and M. Rupp, "Flexible multi-node simulation of cellular mobile communications: the Vienna 5G System Level Simulator," *Eurasip Journal on Wireless Communications and Networking*, 2018.

[8] A. Saleh, A. Rustako, and R. Roman, "Distributed antennas for indoor radio communications," *IEEE Transactions on Communications*, vol. 35, no. 12, pp. 1245–1251, 1987.

[9] H. Osman, H. Zhu, D. Toumpakaris, and J. Wang, "Achievable rate evaluation of in-building distributed antenna systems," *IEEE Transactions on Wireless Communications*, vol. 12, no. 7, pp. 3510–3521, 2013.

[10] H. Hashemi, "Impulse response modeling of indoor radio propagation channels," *IEEE Journal on Selected Areas in Communications*, vol. 11, no. 7, pp. 967–978, 1993.

[11] T. Alade, H. Zhu, and H. Osman, "The impact of antenna selection and location on the performance of DAS in a multi-storey building," in *2013 IEEE Wireless Communications and Networking Conference (WCNC)*, 2013, pp. 3213–3218.

[12] M. Mahbub, M. M. Saym, and M. A. Rouf, "MmWave propagation characteristics analysis for UMa and UMi wireless communications," in *2020 2nd International Conference on Sustainable Technologies for Industry 4.0 (STI)*, 2020, pp. 1–5.

[13] H. Zhu, "Performance comparison between distributed antenna and microcellular systems," *IEEE Journal on Selected Areas in Communications*, vol. 29, no. 6, pp. 1151–1163, 2011.

[14] Y.-H. Nam, B. L. Ng, K. Sayana, Y. Li, J. Zhang, Y. Kim, and J. Lee, "Full-dimension MIMO (FD-MIMO) for next generation cellular technology," *IEEE Communications Magazine*, vol. 51, no. 6, pp. 172–179, 2013.

[15] I. Ahmed, H. Khammari, A. Shahid, A. Musa, K. S. Kim, E. De Poorter, and I. Moerman, "A survey on hybrid beamforming techniques in 5G: Architecture and system model perspectives," *IEEE Communications Surveys Tutorials*, vol. 20, no. 4, pp. 3060–3097, 2018.

[16] T. Lin, J. Cong, Y. Zhu, J. Zhang, and K. Ben Letaief, "Hybrid beamforming for millimeter wave systems using the MMSE criterion," *IEEE Transactions on Communications*, vol. 67, no. 5, pp. 3693–3708, 2019.

[17] X.-H. You, D.-M. Wang, B. Sheng, X.-Q. Gao, X.-S. Zhao, and M. Chen, "Cooperative distributed antenna systems for mobile communications [coordinated and distributed MIMO]," *IEEE Wireless Communications*, vol. 17, no. 3, pp. 35–43, 2010.

[18] MATLAB, *version 9.5.0.944444 (R2018b)*. Natick, Massachusetts: The MathWorks Inc., 2018.

[19] Y. Yuan, *LTE-Advanced relay technology and standardization*. Springer Science & Business Media, 2012.

[20] 3rd Generation Partnership Project (3GPP), "Evolved Universal Terrestrial Radio Access (E-UTRA); Physical layer procedures," 3rd Generation Partnership Project (3GPP), TS 36.213, Jan. 2015.

[21] T. Yoo and A. Goldsmith, "Optimality of zero-forcing beamforming with multiuser diversity," in *IEEE International Conference on Communications, 2005. ICC 2005. 2005*, vol. 1, 2005, pp. 542–546 Vol. 1.

[22] 3rd Generation Partnership Project (3GPP), "Study on channel model for frequencies from 0.5 to 100 GHz (Release 16)," 3rd Generation Partnership Project (3GPP), Tech. Rep. 38.901, 2020.

[23] K. Karakayali, R. Yates, G. Foschini, and R. Valenzuela, "Optimum zero-forcing beamforming with per-antenna power constraints," in *2007 IEEE International Symposium on Information Theory*, 2007, pp. 101–105.

[24] W. Yu and T. Lan, "Transmitter optimization for the multi-antenna downlink with per-antenna power constraints," *IEEE Transactions on Signal Processing*, vol. 55, no. 6, pp. 2646–2660, 2007.

[25] V. U. Prabhu, S. Karachontzitis, and D. Toumpakaris, "Performance comparison of limited feedback codebook-based downlink beamforming schemes for distributed antenna systems," in *2009 1st International Conference on Wireless Communication, Vehicular Technology, Information Theory and Aerospace Electronic Systems Technology*, 2009, pp. 171–176.

[26] K. Satyanarayana, M. El-Hajjar, P.-H. Kuo, A. Mourad, and L. Hanzo, "Millimeter wave hybrid beamforming with DFT-MUB aided precoder codebook design," in *2017 IEEE 86th Vehicular Technology Conference (VTC-Fall)*, 2017, pp. 1–5.

[27] A. Maaref and S. Aissa, "Cross-layer design for MIMO nakagami fading channels in the presence of Gaussian channel estimation errors," in *Canadian Conference on Electrical and Computer Engineering, 2005.*, 2005, pp. 1380–1383.

[28] Y. Chen and N. Beaulieu, "Novel diversity receivers in the presence of Gaussian channel estimation errors," *IEEE Transactions on Wireless Communications*, vol. 5, no. 8, pp. 2022–2025, 2006.

[29] A. D. Dabbagh and D. J. Love, "Multiple antenna MMSE based downlink precoding with quantized feedback or channel mismatch," *IEEE Transactions on Communications*, vol. 56, no. 11, pp. 1859–1868, 2008.

[30] A. Gersho and R. Gray, *Vector Quantization and Signal Compression*, 1991.

[31] C. Bouras, V. Kokkinos, A. Kollia, and A. Papazois, "Techno-economic analysis of ultra-dense and das deployments in mobile 5G," in *2015 International Symposium on Wireless Communication Systems (ISWCS)*, 2015, pp. 241–245.

Table of Abbreviations

BLER Block Error Ratio

BF Beamforming

CQI Channel Quality Indicator

CU Central Unit

DAS Distributed Antenna System

LOS Line-Of-Sight

LTE Long Term Evolution

LTE-A Long Term Evolution - Advanced

MMSE Minimum Mean-Square-Error

MRT Maximum Ratio Transmission

MSE Mean-Square-Error

MU Multi-User

NLOS Non-Line-Of-Sight

RAU Remote Antenna Unit

RF Radio Frequency

SINR Signal-to-Interference-and-Noise-Ratio

SLS Vienna 5G System Level Simulator

SNR Signal-to-Noise-Ratio

SU Single-User

ULA Uniform Linear Array

UMa Urban Macro

VCCS Vienna Cellular Communications Simulators

ZF Zero-Forcing

3GPP 3rd Generation Partnership Project

5G 5th Generation

List of Figures

List of Tables